The Natively Unfolded Character of Tau and Its Aggregation to Alzheimer-like Paired Helical Filaments[†]

Sadasivam Jeganathan,* Martin von Bergen,[‡] Eva-Maria Mandelkow, and Eckhard Mandelkow*

Max Planck Unit for Structural Molecular Biology, Notkestrasse 85, D-22607 Hamburg, Germany

Received May 1, 2008; Revised Manuscript Received July 29, 2008

ABSTRACT: The abnormal aggregation of the microtubule-associated protein Tau into paired helical filaments (PHFs) is one of the hallmarks of Alzheimer disease (AD). Tau in solution behaves as a natively unfolded or intrinsically disordered protein while its aggregation is based on the partial structural transition from random coil to β-structure. Our aim is to understand in more detail the unfolded nature of Tau, to investigate the aggregation of Tau under different conditions and the molecular interactions of Tau in filaments. We show that soluble Tau remains natively unfolded even when its net charge is minimized, in contrast to other unfolded proteins. The CD signature of the random-coil character of Tau shows no major change over wide variations in charge (pH), ionic strength, solvent polarity, and denaturation. Thus there is no indication of a hydrophobicity-driven collapse, neither in the microtubule-binding repeat domain constructs nor in full-length Tau. This argues that the lack of hydrophobic residues but not the net charge accounts for unfolded nature of soluble Tau. The aggregation of the Tau repeat domain (that forms the core of PHFs) in the presence of nucleating polyanionic cofactors (heparin) is efficient in a range of buffers and pH values between ~5 and 10 but breaks down beyond that range, presumably because the pattern of charged interactions disappears. Similarly, elevated ionic strength attenuates aggregation, and the temperature dependence is bell-shaped with an optimum around 50 °C. Reporter dyes ThS and ANS record the aggregation process but sense different states (cross-β-structure vs hydrophobic pockets) with different kinetics. Preformed PHFs are surprisingly labile and can be disrupted by denaturants at rather low concentration (~1.0 M GdnHCl), much less than required to denature globular proteins. Partial disaggregation of Tau filaments at extreme pH values monitored by CD and EM indicate the importance of salt bridges in filament formation. In contrast, Tau filaments are remarkably resistant to high temperature and high ionic strength. Overall, the stability of PHFs appears to depend mainly on directed salt bridges with contributions from hydrophobic interactions as well, consistent with a recent structural model of the PHF core derived from solid state NMR (Andronesi, O. C., von Bergen, M., Biernat, J., Seidel, K., Griesinger, C., Mandelkow, E., and Baldus, M. (2008) Characterization of Alzheimer's-like paired helical filaments from the core domain of tau protein using solid-state NMR spectroscopy. *J. Am. Chem. Soc. 130*, 5922−5928).

Tau is a microtubule-associated protein (MAP) that functions primarily to stabilize microtubules in the axons of neurons. Microtubules in turn provide the tracks for motor proteins and thus allow intracellular transport of vesicles, organelles, and protein complexes by motor proteins (for review, see ref *2*). Tau in solution behaves as a random coil, as judged by electron microscopy, X-ray diffraction, CD,[1] FTIR, fluorescence spectroscopy and other methods (for review, see ref *3*). The repeat domain of Tau (Figure 1A) is central both for microtubule binding and for the pathological aggregation of Tau in Alzheimer disease. The two hexapeptide motifs in repeats R2 and R3 can undergo a conformational change from random coil to β-structure and thus act as seeds for aggregation (*4*, *5*). Analysis of repeat domain constructs by NMR spectroscopy confirmed the overall paucity of secondary structural elements, but also confirmed the β-structure propensity in the repeat domain (*6*−*8*).

The lack of structure in natively unfolded proteins is hypothesized to be due to their low content of hydrophobicity and a high net charge near physiological pH (*9*). Indeed, the primary sequence of Tau has a low hydrophobic content (mean hydrophobicity = 0.404) but a net charge of only +2 (mean net charge = 0.005). For some of the natively

[†] This project was supported in part by grants from the Deutsche Forschungsgemeinschaft and the Volkswagen Foundation.

* Corresponding authors. Tel: +49-40-89982810. Fax: +49-40-897168. E-mail: siva@mpasmb.desy.de and mand@mpasmb.desy.de.

[‡] Present address: Helmholtz Centre for Environmental Research-UFZ, Department of Proteomics, Permoserstr. 15, D-04318 Leipzig, Germany.

[1] Abbreviations: AD, Alzheimer disease; PHF, paired helical filaments; EM, electron microscopy; CD, circular dichroism; NMR, nuclear magnetic resonance; FTIR, Fourier transform infrared; GdnHCl, guanidine hydrochloride; ThS, thioflavin S; ANS, 8-anilino-1-naphthalenesulfonate; PPII, poly proline II helix; p*I*, isoelectric point; PBS, phosphate buffered saline; NH_4Ac, ammonium acetate; BES, *N*,*N*-bis(2-hydoxyethyl)-2-aminoethanosulfonic acid; Bis Tris, bis-(2-hydroxylmethyl)-imino (hydroxymethyl)-methane; CAPS, 2-(*N*-cyclohexylamino)-1-propanesulfonic acid; CHES, 2-(*N*-cyclohexylamino)ethanesulfonic acid; HEPES, *N*-2-hydroxyethyl-piperazine-*N*-2-ethanesulfonic acid; MES, 2-(*N*-morpholino)ethanesulfonic acid; MOPS, 2-(*N*-morpholino)-propanesulfonic acid; NaAc, sodium acetate; NaP, sodium phosphate; PIPES, piperazine-*N*,*N*′-bis-(2-ethanesulfonic) acid; Tris, tris-(hydroxylmethyl)-aminomethane.

10.1021/bi800783d CCC: $40.75
Published on Web 09/11/2008

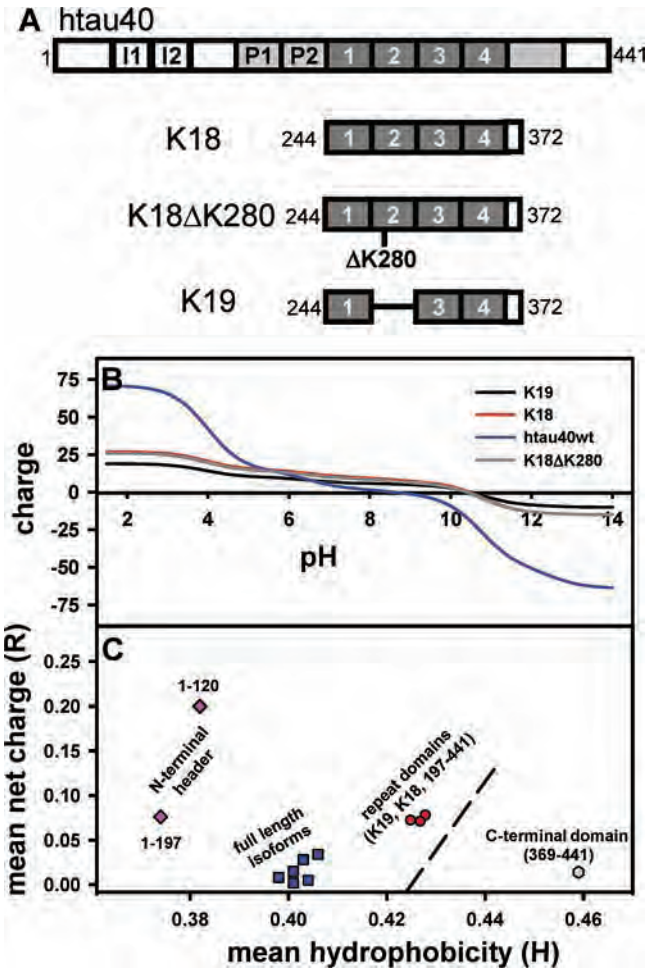

FIGURE 1: Tau constructs and pH dependent net charge. (A) Bar diagrams showing full length isoform hTau40wt and Tau constructs: K19, K18 and K18ΔK280. (B) The change of net charge of Tau constructs and isoform with respect to pH was predicted by the EMBOSS IEP program (*21*). The repeat-domain constructs (K19, K18, K18ΔK280) have similar isoelectric points (around 10.5), reflecting their basic nature. Full-length Tau (hTau40) has a p*I* of 8.61 which results from the combination of basic and acidic domains. At pH 7, the net charge and isoelectric point of the repeat domain constructs is +7 and 10.49 (K19), +10 and 10.46 (K18ΔK280), +9 and 10.39 (K18), whereas for full-length Tau it is much lower, +2 and 8.6 (hTau40). (C) Mean net charge and mean hydrophobicity of Tau isoforms (blue squares) and Tau repeat constructs (red circles). The dashed line represents the border between intrinsically disordered and folded proteins (*9*). Note that only the C-terminal tail of Tau (gray hexagonal), taken by itself, is predicted to contain appreciable secondary structure (due to its amphipathic α-helical character).

unfolded proteins, it has been shown that either the minimization of the net charge by varying the pH of the solvent or elevated temperature can induce partial folding to a partially folded intermediate by permitting hydrophobicity-driven collapse (*9*).

Natively unfolded proteins are thought to adopt some structure upon binding to their partners (*10*), but this issue is not clear for Tau. Some authors have postulated several conformations upon binding to microtubules (*11*) whereas other results indicated that Tau retains much of its disordered state on the microtubule surface (*12*, *13*). NMR analysis of Tau−microtubule interactions highlighted binding of several stretches of positively charged amino acids present in the repeat domains and the flanking regions to microtubules without specifying a structural transition (*6*, *7*). Independently of conformation, the microtubule-binding domain becomes immobilized on the microtubule surface, whereas the majority of the N-terminal and C-terminal domains remain disordered and do not contribute to microtubule binding either (*14*, *15*).

Even though Tau is highly soluble, it can be induced to aggregate in vitro. The major contribution comes from the repeat domain which nucleates PHFs; this can be enhanced by oxidation and by polyanionic cofactors which compensate Tau's positive charges (*16*−*19*). Nevertheless, the conditions and triggers for the aggregation of Tau are still poorly understood, both in vitro and in cells.

In this study, we have therefore investigated the determinants of the unfolded nature of soluble Tau, the biochemical parameters that govern the aggregation of Tau and of the stability of Tau filaments under different solution conditions such as varying pH, temperature, salt and organic solvents using biochemical and biophysical techniques. We show that the unfolded nature of Tau can be attributed mostly to the lack of hydrophobicity and that aggregation is largely determined by ionic interactions.

MATERIALS AND METHODS

Chemicals and Proteins. Heparin (average MW of 3000 or 6000 Da), GdnHCl and ThS were purchased from Sigma (Munich, Germany). Full-length Tau isoform hTau40 and Tau constructs K19, K18 and K18ΔK280 (Figure 1A) were expressed in *E. coli* and purified by heat treatment and FPLC Mono S chromatography (Amersham Pharmacia, Freiburg) as described previously (*20*). The purity of the proteins was analyzed by SDS−PAGE, and the protein concentrations were determined by absorbance at 214 nm.

CD Spectroscopy. All measurements were carried out with a Jasco J-810 CD spectrometer (Jasco, Gross-Umstadt, Germany) in a cuvette with a path length of 0.1 cm. The parameters were scanning speed, 100 nm/min; bandwidth, 0.1 nm; response time, 4 s; measurement temperature, 20 °C. The CD spectra were normalized for concentration at 214 nm using BSA as standard. In each experiment, 3 spectra were summed and averaged. For the measurements of PHFs in denaturant GdnHCl, a cuvette with 0.01 cm path length was used. Due to the high absorbance of GdnHCl near 200 nm which impairs the quality of CD signal, the 205/217 intensity ratio was used for the interpretation of the results.

PHF Assembly. Aggregation was induced by incubating soluble Tau or Tau constructs typically in the range of 50 μM in volumes of 20 μL at 37 °C in different buffers with or without the anionic cofactor heparin 3000 or 6000 (molar ratio of Tau to heparin = 4:1) for incubation times of ∼3 days. The formation of aggregates was monitored by ThS fluorescence and electron microscopy. Buffers used for optimizing the aggregation conditions are at 20 mM concentration unless stated otherwise, and the ionic strength of the buffer is given in the parentheses: sodium phosphate pH 2 (0.008 M), sodium phosphate pH 3 (0.017 M), sodium citrate pH 3.5 (0.024 M), sodium acetate pH 4 (0.003 M), sodium acetate pH 5 (0.013 M), sodium citrate pH 5.5 (0.043 M), MES pH 5.5 (0.003 M), sodium phosphate pH 6 (0.022 M), BES pH 6.4 (0.002M), Bis Tris pH 6.4 (0.01 M), sodium citrate pH 6.4 (0.056 M), MES pH 6.4 (0.013 M), MOPS

pH 6.4 (0.002 M), PIPES pH 6.4 (0.03 M), HEPES pH 6.8 (0.002 M), sodium phosphate pH 7 (0.041 M), PBS pH 7.4 (0.16 M), BES pH 7.4 (0.013 M), Bis Tris pH 7.4 (0.001 M), HEPES pH 7.4 (0.008 M), MOPS pH 7.4 (0.012 M), PIPES pH 7.4 (0.052 M), Tris pH 7.4 (0.02 M), sodium phosphate pH 8 (0.057 M), MOPS pH 8 (0.017 M), sodium phosphate pH 8 (0.057 M), HEPES pH 8.2 (0.016 M), Tris pH 8.2 (0.007 M), sodium carbonate pH 9 (0.01 M), CHES pH 9 (0.006 M), Tris pH 9 (0.001 M), sodium carbonate pH 10 (0.021 M), CAPS pH 10 (0.005 M), CHES pH 10 (0.016 M), sodium carbonate pH 11 (0.028 M); CAPS pH 11 (0.016 M), sodium phosphate pH 12 (0.102 M).

ThS Fluorescence. Five microliters of 50 μM assembly reactions were diluted to 50 μL with NH_4Ac pH 7 containing 20 μM ThS. Then ThS fluorescence was measured in a Tecan spectrofluorimeter (Crailsheim, Germany) with an excitation wavelength of 440 nm and an emission wavelength of 521 nm (slit width 7.5 nm each) in a 384 well plate (black microtiter 384 plate round well; Thermo Labsystems, Dreieich, Germany). Measurements were carried out at 25 °C, and the background fluorescence was subtracted when needed.

ANS Fluorescence. Five microliters of 50 μM assembly reactions were diluted to 50 μL with NH_4Ac pH 7 containing 100 μM ANS. All ANS fluorescence experiments were carried out in a Tecan spectrofluorimeter at 25 °C using an excitation wavelength of 375 nm and an emission wavelength of 490 nm (slit width 7.5 nm each). In the denaturation experiments, the effect of GdnHCl concentrations on the fluorescence of free ANS was subtracted (10−15%, depending on the concentration).

Electron Microscopy. Protein solutions were diluted to 1−10 μM and placed on 600 mesh carbon coated copper grids for 45 s, washed twice with H_2O, and negatively stained with 2% uranyl acetate for 45 s. The samples were examined with Philips CM12 electron microscope at 100 kV.

RESULTS

A. Structure of Tau in Solution. Tau has a physiological role as a microtubule stabilizing molecule and pathological role as it aggregates into PHFs in AD. Tau is considered as a natively unfolded protein which lacks a significant amount of secondary structure, as judged by a variety of biophysical criteria. Proteins of this class are often characterized by a high net charge at physiological pH and by a low hydrophobicity (*9*). All of the Tau isoforms and constructs contain numerous charged residues (e.g., hTau40 contains 27 E, 29 D, 44 K, 14 R, 12 H, together ∼29% of all residues). Negative charges dominate the N-terminal header which includes the two inserts (up to residue 120), whereas the remainder is dominated by positively charged residues. Thus all Tau proteins have an overall basic character. At neutral pH the net charge of full-length isoform hTau40 and Tau constructs K19, K18, K18ΔK280 (which represent part of microtubule binding region and include the region forming the core of PHFs) (Figure 1A) is +2 and +7, +10, +9 respectively and the isoelectric point (p*I*) is 8.6 and 10.49, 10.46, 10.39 respectively as predicted by the "EMBOSS IEP" program (*21*) (Figure 1B). The full length isoform hTau40 fulfills one of the criteria of natively unfolded proteins by having a low hydrophobicity (mean hydrophobicity, H = 0.428, computed according to FoldIndex (*22*) where hydrophobicity values are normalized to lie between −1 and +1). Nevertheless, the net charge is surprisingly low, only +2. This implies a low mean net charge, R, of 2/441 = 0.005, compared with values ∼0.12 for other natively unfolded proteins (*9*). However, this value of net charge disguises the fact that Tau is a multidomain protein with each domain carrying a different high net charge (Figure 1C). This holds particularly true for the repeat domains. The repeat domains exhibit a mean hydrophobicity of 0.43 and a high net charge of +9 (mean net charge = 0.072) that are consistent with values predicted for natively unfolded protein. This prompts the question of whether a high net charge is a necessary condition for a natively unfolded protein. This can be tested, for example, by minimizing the net charge through a variation of the pH. On the other hand, treatment at elevated temperature has been reported to induce partial folding by causing a hydrophobicity-driven collapse in some unfolded proteins (e.g., α-synuclein) that are otherwise unfolded at room temperature due to low content of hydrophobic amino acids (*23*). We therefore used hTau40 and the repeat domain constructs (K19, K18, K18ΔK280) to test the structural transitions against variations of solvent conditions. The repeat domain constructs K19 and K18 (corresponding to fetal or adult Tau) represent the central part of microtubule binding region, which coincides with the region responsible for forming PHFs. The mutation ΔK280 is one of the mutations that occur in Frontotemporal dementia with Parkinsonism linked to chromosome -17 (FTDP-17). This mutation of Tau shows faster PHF assembly kinetics and causes a higher stability of PHFs, which is explained by the formation of a larger amphipathic patch around the nucleating hexapeptide motif PHF6* (*4*, *24*). The properties of the proteins in the soluble state were monitored by different types of spectroscopy (CD, FTIR, NMR, X-ray, complemented by electron microscopy). For the variations of solvent conditions and effects on secondary structure reported here we rely mainly on CD spectroscopy to monitor the effects of pH, temperature, ionic strength, and solvents.

1. pH Dependence. The effect of minimizing the net charge of Tau on its secondary structure was analyzed by incubating soluble Tau at different pHs and recording their CD spectra. Figure 2A shows the CD spectra of K19 recorded at different pH values; they all showed a minimum at ∼200 nm indicating a mostly random coil conformation. The spectra of K19 indicated no increase in secondary structure in the pH range 9 to 12 at which net charge of K19 is minimized. To illustrate this more clearly, we plotted the ratio of the ellipticity at 200 nm (indicative of random coil) and at 217 nm (sensitive to β-structure) against pH. There was only a small change at any pH even though charge neutralization occurs around pH 10 (Figure 2B). A similar lack of significant change against varying pH was observed for other Tau constructs such as K18, K18ΔK280 or full length isoform hTau40 (Figure 2B). This indicates that the additional repeat R2, the N-terminal half or the C-terminal tail did not alter the average conformation. We conclude that the failure of Tau to fold partially even when the charge is neutralized can be attributed to its very low hydrophobic content which is not sufficient for a hydrophobicity-driven collapse. In this regard, Tau appears similar to the natively unfolded protein securin, with values for H = 0.45, R = 0.05 and pI = 6.2, whose structure is unaltered as a function

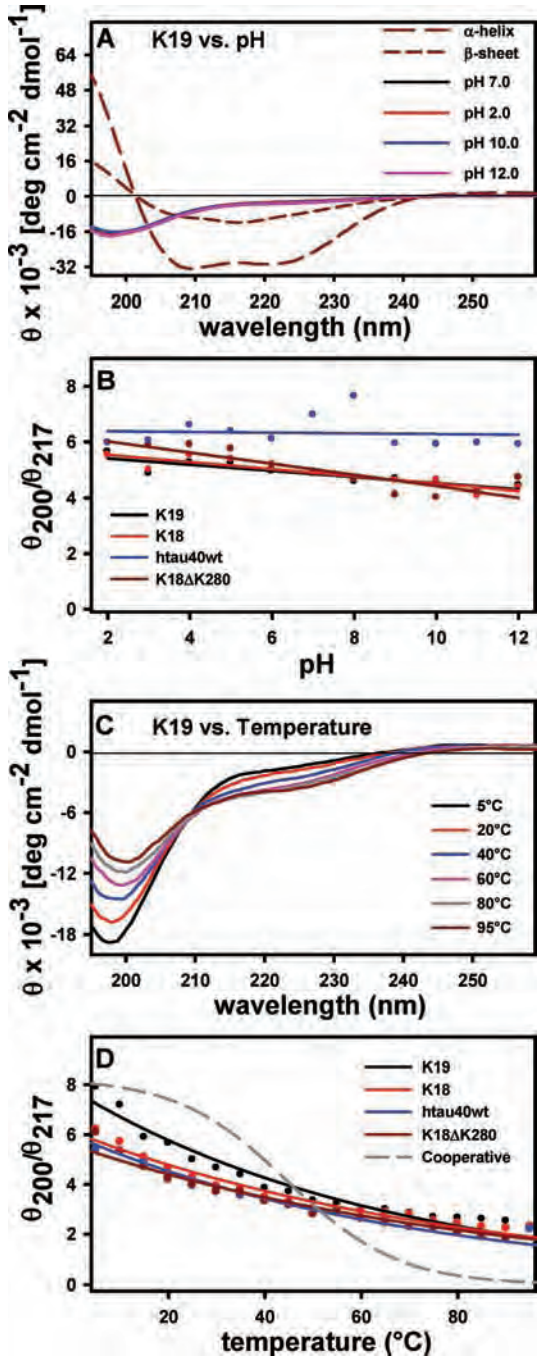

FIGURE 2: CD spectra of Tau as a function of pH and elevated temperature. (A) CD spectra of K19 at pHs 7, 2, 10 and 12 are shown. CD signature of α-helix and β-sheet are also shown. (B) 200/217 nm ratio of CD spectra obtained at each pH for K19, K18, hTau40wt and K18ΔK280 are plotted against pH. Note that the spectra do not indicate a significant structural change in Tau with change of pH and the 200/217 nm ratio shows only small changes in the pH range 4−6. (C) CD spectra of K19 at different temperatures: 5 °C, 20 °C, 40 °C, 60 °C, 80 °C and 95 °C. Note the significant reduction of the negative peak at 200 nm. (D) 200/217 nm ratio of K19, K18, hTau40wt and K18ΔK280 at various temperatures, showing a strong decrease from ∼7 to 2. However, the transition does not occur in a cooperative fashion (shown as dashed line), indicating that there is a lack of hydrophobic residues to collapse into a hydrophobic core. In addition, temperature dependent CD spectra of Tau are similar to that of polyproline II helix (PPII). Thus the transition of Tau from the semiextended PPII state to a more extended conformation would also explain the spectral change upon temperature rise. CD data were obtained at 20 °C with a 0.1 cm cuvette; scanning speed 100 nm/min; bandwidth 0.1 nm; response time 4 s.

of pH (*25*). In contrast, α-synuclein ($H = 0.454$, $R = 0.055$ and p$I = 4.44$) showed a well-defined structural transition between pH 2 and 8, suggestive of a transition from the natively unfolded state to a partially folded intermediate (*23*), likely due to the presence of the hydrophobic nonamyloid component (NAC) region.

2. Temperature Dependence. To test if elevated temperature could cause a structural transition, the secondary structure of soluble Tau was determined by CD at various temperatures (from 5 to 95 °C). Upon stepwise elevation of temperature, the CD spectra of K19 underwent a shift: the (negative) peak at 200 nm became less pronounced and the value at 217 nm became more negative, with an isobestic point around 210 nm (Figure 2C). However, the 200/217 nm ratio showed a uniform change (Figure 2D), typical of a simple two-state system (indicated by isobestic point around 210 nm) rather than a sigmoidal transition which is a signature for cooperative folding (*26*). The same behavior was observed for K18, K18ΔK280 and hTau40wt (Figure 2D). Thus, the absence of cooperative folding appears to be due to the low fraction of hydrophobic residues and is shared by all domains of Tau tested. Second, a red shift of only ∼2 nm from the minimum at ∼196 nm was observed upon temperature elevation. This suggests that the transition observed with temperature rise is minimal, because any substantial transition from random coil to α-helix or β-structure would result in a large red shift (from ∼200 nm to ∼217 nm). Third, we note that proteins or peptides containing a large fraction of polyproline helix II (PPII) show a similar temperature dependent CD which can be explained by a gradual change from a conformation rich in PPII to more extended conformations (*25, 27*).

3. Ionic Strength. The effects of salts on protein structure are mainly due to changes in the interactions with the solvent water, such as H-bonding between water molecules, solvent to protein side chains and protein backbone. Thus the salt ions might lead to an increase or decrease in the hydrophobic interactions of proteins and can destabilize the salt bridges by masking charged residues. For natively unfolded proteins, salt ions might lead to an increase in the hydrophobic interactions by shielding the charged residues. To check if any changes take place in the structure of Tau upon increased salt concentrations, Tau constructs were investigated by CD at various salt concentrations (0−750 mM Na_2SO_4). There was no indication of structural changes for K19, K18 and hTau40wt although K18ΔK280 showed slightly higher change (Figure 3A,B). The inability of salt to induce any ordered structure speaks for the low hydrophobic content of Tau as a primary reason for the unfolded nature.

4. Polarity of Solvent. The effect of alcohols such as TFE, HFIP, ethanol, methanol, isopropanol is considered to arise from the low solvent polarity. For example, TFE reduces the interaction between water molecules and protein, and therefore allows the protein to unravel and make intramolecular hydrogen bonds (leading to formation of α-helix) (*28*). Thus TFE initially induces unfolding of globular proteins to a partially folded state and then induces α-helix formation in unfolded regions. For natively unfolded proteins, TFE promotes secondary structure since the polypeptide backbone is exposed already. The structure of Tau was investigated by CD at various concentrations of isopropanol (0−25%) in order to test the influence of solvent polarity.

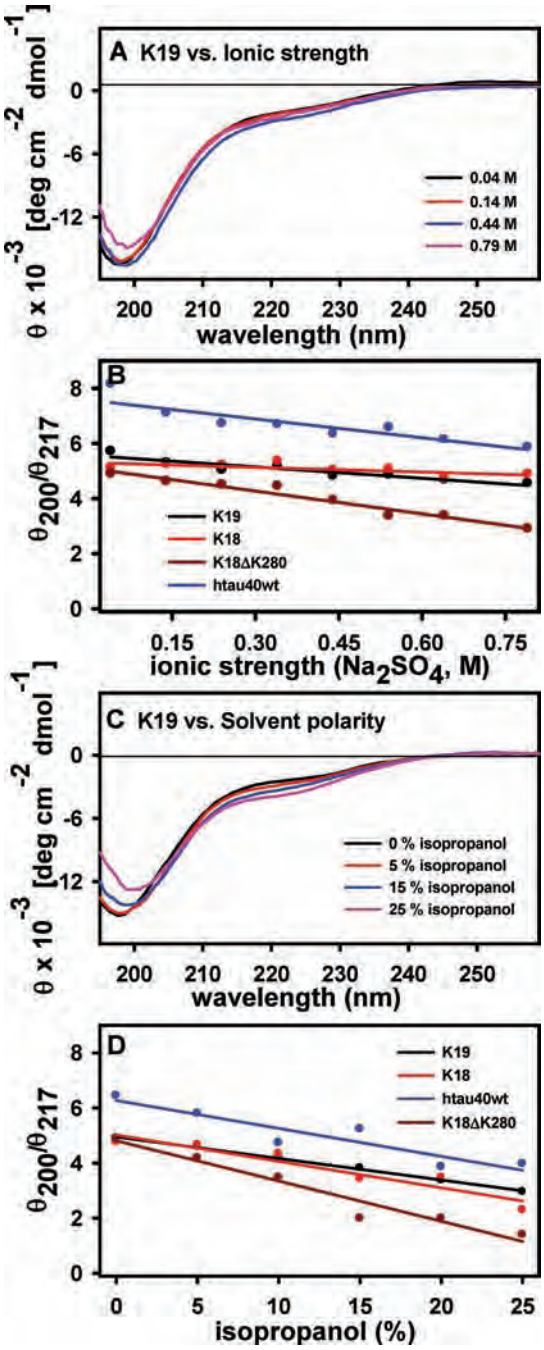

FIGURE 3: CD spectra of soluble Tau vs ionic strength and solvent polarity. (A) CD spectra of K19 at ionic strengths 0.04 M, 0.14 M, 0.44 and 0.79 M are shown. The ionic strength given includes the basic ionic strength of phosphate buffer (0.04 M) and the salt-Na_2SO_4 added. (B) 200/217 nm ratio of K19, K18, hTau40wt and K18ΔK280 at various concentrations of added salt. Note that Tau secondary structure is not altered by high salt concentration. (C) CD spectra of K19 vs solvent polarity by adding different concentrations of isopropano,l 0%, 5%, 15% and 25% (corresponding to the dielectric constant of the solvent from 80 to 65), are shown. (D) 200/217 nm ratio of K19, K18, hTau40wt and K18ΔK280 at various isopropanol concentrations. Note that alcohol alters slightly the Tau structure though much of randomness remained at the alcohol concentrations used here. Secondary structure estimation using software based on Yang et al. (*65*) revealed 60% random, 18% turn, 22% β-sheet and 0% α-helix in the absence of alcohol compared to 54% random, 7% turn, 39% β-sheet and 0% α-helix in the presence of 25% alcohol for K19. Alcohol is known to disrupt the H-bonding between protein and water, thus favoring formation of intramolecular H-bonding within protein. Conditions for the measurements were the same as in Figure 2.

The dielectric constant of water is 80, and that of isopropanol is 18; thus a change from 0 to 25% isopropanol corresponds to a dielectric constant change from 80 to 65. Treatment with 0−25% isopropanol showed only a slight effect on the structure of Tau (Figure 3C,D). Thus, the decreasing dielectric constant did not have a dramatic effect on the unfolded nature of soluble Tau.

B. Aggregation of Tau into PHFs. The aggregation of soluble Tau into filaments in vitro is intrinsically very slow but can be enhanced by the addition of polyanions (*16*, *18*). It is believed that polyanions favor aggregation by neutralizing the positive charges in the repeat region of Tau. We investigated the conditions that influence the aggregation by incubating Tau at various pH values in different types of buffer, in a range of ionic strength and temperature values. Tau constructs K19 and K18 that form the PHF core region were used for optimizing the conditions, and the aggregation was monitored by the fluorescent reporter dyes Thioflavin S (ThS) and 8-anilino-1-naphthalenesulfonate (ANS).

1. Charge Neutralization Favors Aggregation. We first examined the aggregation of Tau constructs K19 (net charge = +7 and p*I* = 10.49) at different pH values. The polymerization reactions were set up with 50 μM K19 in the presence or absence of the polyanion heparin 3000 (molar ratio of heparin:protein = 1:4) in various buffers in the pH range 2−12 with incubation times of 3 days. The extent of polymerization was determined by ThS fluorescence, and the presence of filaments was ascertained by electron microscopy (EM). Figure 4A shows the ThS fluorescence as a measure of the aggregation efficiency of K19. It indicates that aggregation efficiency was low at pH values <5; moderate between pH 6 and 8, highest between pH 8−10; and again low at pH values >10. The high efficiency of K19 aggregation just below its isoelectric point (=10.49) in the presence of heparin indicates that the minimization of net charge favors the aggregation (Figure 4B). However, the presence of the cofactor heparin was found to be necessary even around pH values near its p*I* and the aggregation of K19 at pH > 10 was low even in the presence of heparin (Figure 4B). This points to the fact that heparin not only is important for shielding the repulsive charge but also might have an additional effect. The electron micrographs of filaments formed at pH 10 closely resemble the morphology of typical PHFs (Figure 4C). A similar pattern of aggregation efficiency was observed for the construct K18, also exhibiting slightly better aggregation efficiency around pH 10 (Figure S1A,B in the Supporting Information). The morphology of filaments was similar to those obtained around neutral pH (Figure S1C in the Supporting Information). The observation that charge minimization of Tau increases aggregation is consistent with other unfolded proteins. For example, α-synuclein (p*I* = 4.44) aggregates faster at low pH, probably due to the induction of a partially folded conformational state (*23*). However, it should be noted that the aggregation of Tau depends on its charge neutralization by polyanionic cofactors (e.g., heparin) whereas the aggregation of α-synuclein is self-driven. In contrast, many globular proteins are also shown to aggregate at extreme pHs due to the destabilization of the folded state toward partially folded intermediates (*29*).

2. Increasing Ionic Strength Reduces Aggregation. The effect of ionic strength on the aggregation of K19 was examined by carrying out the polymerization in the presence

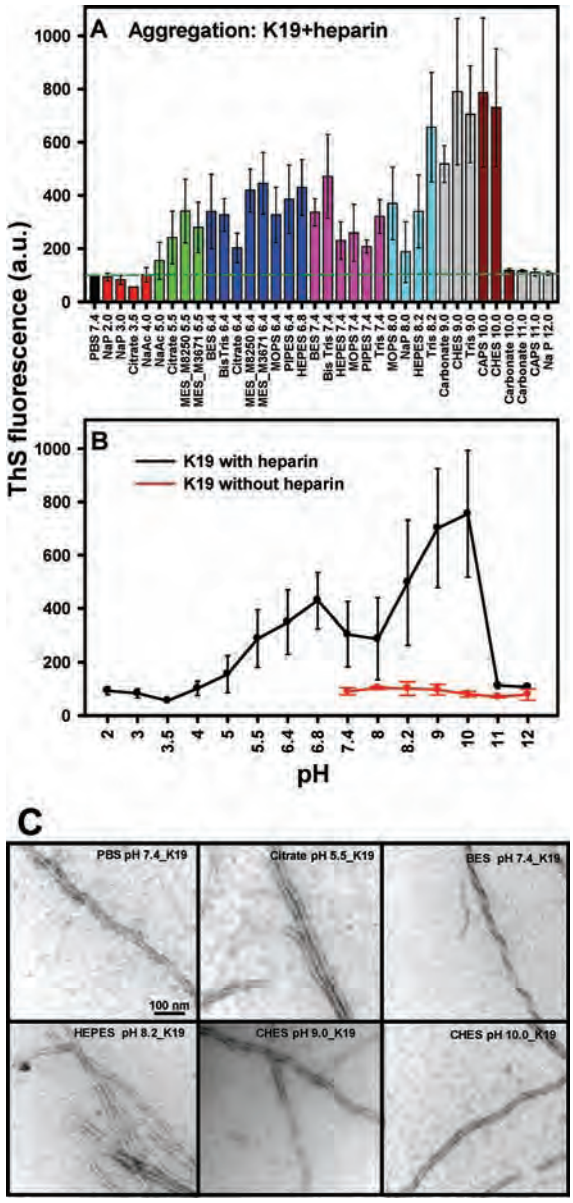

FIGURE 4: Aggregation of K19 at different pH values and electron micrographs of K19 filaments. (A) ThS fluorescence profile of polymerization reactions of K19 at different pH values. The aggregation was induced from 50 μM K19 protein in 20 mM buffer of different pH values in the presence or absence of heparin 3000 (molar ratio of Tau:heparin = 4:1) and incubated at 37 °C for 3 days. The extent of aggregation was then measured by ThS fluorescence by taking 5 μL of 50 μM assembly reactions diluted to 50 μL with NH_4Ac pH 7 containing 20 μM ThS. Fluorescence measurements were done at 25 °C with an excitation wavelength of 440 nm and an emission wavelength of 521 nm (slit width 7.5 nm each) in a 384 well plate. The background fluorescence was subtracted when needed, and the fluorescence intensity of assembly reactions in the different buffers was normalized to fluorescence of reaction in PBS pH 7.4 (set as 100%). Note that the K19 aggregation is significantly higher at pH values just below its isoelectric point, except in carbonate buffer, probably due to its weak buffering capacity. (B) The average fluorescence intensity of the polymerization reaction in all buffers of each pH value. Note that Tau aggregation requires the presence of heparin even at pH values that minimize the charge. (C) Electron micrographs of K19 filaments in different conditions of buffer and pH. An aliquot of a K19 aggregation sample was loaded on 600 mesh copper grid, washed twice with water and then stained with 2% uranyl acetate. The grids were checked for the presence of filaments in a Philips CM12 transmission microscope. The scale bar represents 100 nm and is the same for all the pictures.

of heparin 3000 in a buffer of increasing salt concentrations (0−500 mM NaCl) with incubation of 3 days. ThS fluorescence indicates that the aggregation efficiency of K19 was strongly attenuated with increasing ionic strength (Figure 5A). A similar pattern was observed for K18 (Figure S2A in the Supporting Information), in good agreement with an earlier study (*30*). Tau aggregation in the presence of anionic cofactors is based on dimerization and subsequent addition of Tau molecules (*17*, *31*). The salt dependence of Tau aggregation suggests an ionic nature for the interaction between Tau and heparin or between Tau molecules, since salt can affect the interaction between water and protein side chains or backbone by masking charged residues. For comparison, the aggregation of α-synuclein and β2-microglobulin is increased in the presence of salt due to either a change of protein−water interaction or preferential anion binding to the protein (*32*, *33*).

3. Temperature Optimum for Aggregation. We then analyzed the effect of increasing temperature on K19 aggregation. Polymerization reactions were set up with 50 μM K19 in the presence of heparin 3000 and incubated at various temperatures (25−80 °C) for 3 days. ThS measurements of these assembly reactions were done in standard conditions immediately after cooling down the reactions to 25 °C. The aggregation efficiency of K19 increased up to 50 °C but decreased again at 70 and 80 °C as evidenced from the ThS fluorescence intensity measurement (Figure 5B). A similar behavior was found for the aggregation of K18 (Figure S2B in the Supporting Information). Thus the aggregation of Tau showed two phases upon temperature rise. Increasing the temperature weakens several types of interactions of proteins, particularly the mobilization of clathrate water structure around monomeric proteins. This is compensated by burying interaction surfaces, e.g. hydrophobic interactions. In addition the formation of salt bridges is favored at high temperature due to the decrease of the electrostatic desolvation penalty of salt bridges (*34*). Hence efficient aggregation of Tau up to 50 °C should be partially entropy-driven, as a result of favoring salt bridge formation and hydrophobic interactions between Tau molecules. On the other hand, the drop in aggregation above 50 °C can be explained by the prevention of H-bonding between backbones of Tau molecules or interactions between Tau and heparin, possibly due to the kinetic energy provided by the high temperature. In comparison, the aggregation of α-synuclein was also shown to increase at high temperatures, probably due to the formation of a partially folded intermediate (likely by hydrophobic NAC region) which is more prone for aggregation than the native state (*23*). Similar to a two-phase model of temperature dependent Tau aggregation, insulin aggregation showed a threshold temperature of 80 °C. This behavior of insulin can be explained due to the transition of monomeric insulin (α/β) to a partially folded intermediate prone to faster aggregation up to 80 °C, whereas beyond 80 °C there is a transition to the random coil state that fails to undergo aggregation (*35*).

4. Monitoring Aggregation by ANS vs ThS Fluorescence. Hydrophobic patches are known to contribute to pathological aggregation of disease related proteins and are often located at the core of the fibrils (*29*). To check whether there is an increased hydrophobicity in the case of PHFs, ANS was used to monitor the aggregation, in parallel with the fluorescence

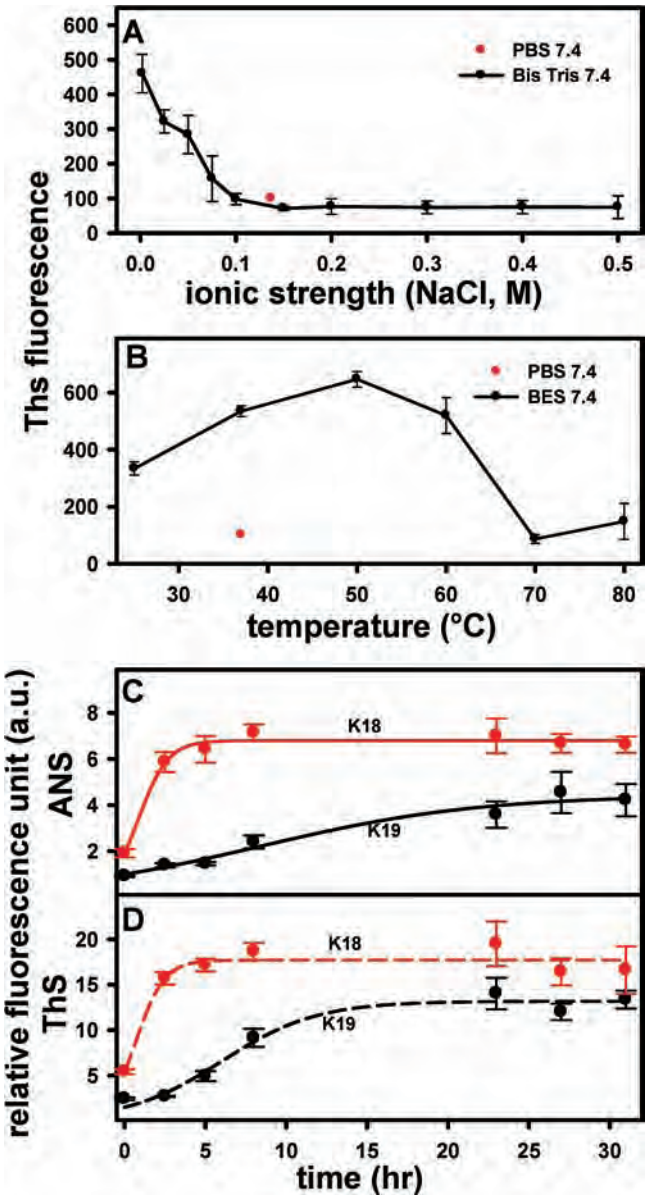

FIGURE 5: Aggregation efficiency of K19 vs ionic strength and temperature. (A) ThS fluorescence profile of polymerization reactions of K19 at various salt concentrations. Aggregation was induced from 50 μM protein in 20 mM BisTris pH 7.4 buffer (ionic strength due to this buffer = 0.001 M) plus various salt concentration with addition of heparin 3000 (molar ratio of Tau:heparin = 4:1) and incubated at 37 °C for 3 days. ThS fluorescence was measured in standard conditions as in Figure 4. Note that the aggregation becomes very inefficient at ionic strengths above 0.1 M. (B) Polymerization reactions of K19 at various temperatures. Aggregation was set up by taking 50 μM protein in 20 mM BES pH 7.4 in the presence of heparin 3000 (molar ratio of protein:heparin = 4:1), incubated at different temperatures for 3 days and then quantified by ThS fluorescence. Note that aggregation has a broad optimum around 50 °C but drops off steeply at 70 °C and above. (C and D) Aggregation of K19 and K18 monitored by the fluorescence of ANS (C) and Thioflavin S (D). Aggregation was started with 50 μM protein in the presence of heparin 6000 (molar ratio of Tau:heparin = 4:1) and incubated at 37 °C. Five microliters of PHF reaction was diluted to 50 μL with NH_4Ac pH 7 containing 100 μM ANS or 20 μM ThS. ANS fluorescence was observed using excitation at 375 nm and emission 490 nm (slit width 7.5 nm each) at 25 °C and ThS fluorescence measured as described in Figure 4. The aggregation of K19 and K18 monitored by ANS fluorescence is shown (solid black and red lines respectively). Note that the increase of ANS and ThS fluorescence is equivalent as the aggregation proceeds, with K18 aggregating faster than K19 confirming the formation of hydrophobic pockets.

of ThS. ANS binds to solvent-exposed hydrophobic pockets that are generated by aggregation, resulting in an increase in fluorescence intensity (*36*). Figure 5C shows that the ANS fluorescence increased as polymerization proceeded, indicating that hydrophobic binding sites are created. The fluorescence of ThS fluorescence, thought to be indicative of β-structure, showed a similar time course (Figure 5D), and the EM analysis confirmed aggregation into PHFs (data not shown). Thus the data argue that the formation of hydrophobic pockets parallels the buildup of β-structure in the filaments. The aggregation of hTau40 did not show higher ANS fluorescence (Figure S2C in the Supporting Information) than aggregation of K19 or K18, indicating that the increased hydrophobic pockets are confined to the repeat domains.

C. Structural Properties of PHFs. Tau aggregation is similar to that of other amyloidogenic proteins with regard to the generation of cross β-structure. However, the molecular details on how this β-structure arises from the natively unfolded state are not known. To further understand the factors contributing to stability, PHFs derived from K19, K18 and K18ΔK280 were subjected to various conditions such as pH, temperature, or denaturation in GdnHCl and monitored spectroscopically and biochemically.

1. PHFs Are Highly Sensitive to Denaturation. Denaturation by GdnHCl is often used to probe the stability of proteins. The mechanism of denaturation by GdnHCl is thought to be due to the increased solubility of most groups compared to water, thus stabilizing the more solvent-exposed unfolded state relative to the native state (*37*). An additional factor is the weak binding of GdnHCl to the polypeptide backbone, thus disturbing backbone hydrogen bonds (*38*). Thus GdnHCl can disrupt both hydrophobic and ionic interactions to cause denaturation. Using tryptophan scanning mutagenesis, we showed that PHFs can be unexpectedly labile (*24*). We therefore investigated the structural changes of PHFs preassembled in standard conditions (heparin 6000, incubation at 37 °C for ~3 days), during GdnHCl-induced denaturation using CD. With increasing concentration of GdnHCl, the negative ellipticity of K19-PHFs shifted from 217 to 200 nm indicating a change from β-structure to random coil during dissolution (Figure 6A). The plot of 205/217 nm ratio confirmed the structural transition from β-structure to random coil with midpoints at relatively low concentrations of GdnHCl, around 0.5 M for K19-PHFs and 1 M for K18-PHFs (Figure 6B), indicating that overall both types of filaments are remarkably labile, and that the additional repeat of K18 provides additional stability of the PHFs. For K18ΔK280-PHFs the midpoint is much higher, ~4 M (Figure 6B), comparable with the stability of typical folded proteins. This illustrates that the FDTP-17 mutation ΔK280 has a major effect on PHF stability which is likely explained by the increased amphipathic β-structure by deletion of K280 (*4*). To validate the results obtained by CD, the ANS fluorescence of PHFs was measured in the presence of GdnHCl. Denaturation resulted in a loss of fluorescence, concomitant with the disappearance of the hydrophobic binding pockets in PHFs. The curves showed midpoints around 0.5 M for K19-PHFs, 0.8 M for K18-PHFs and 2 M GdnHCl for K18ΔK280-PHFs (Figure 6C). These values were lower than those of the CD experiments consistent with

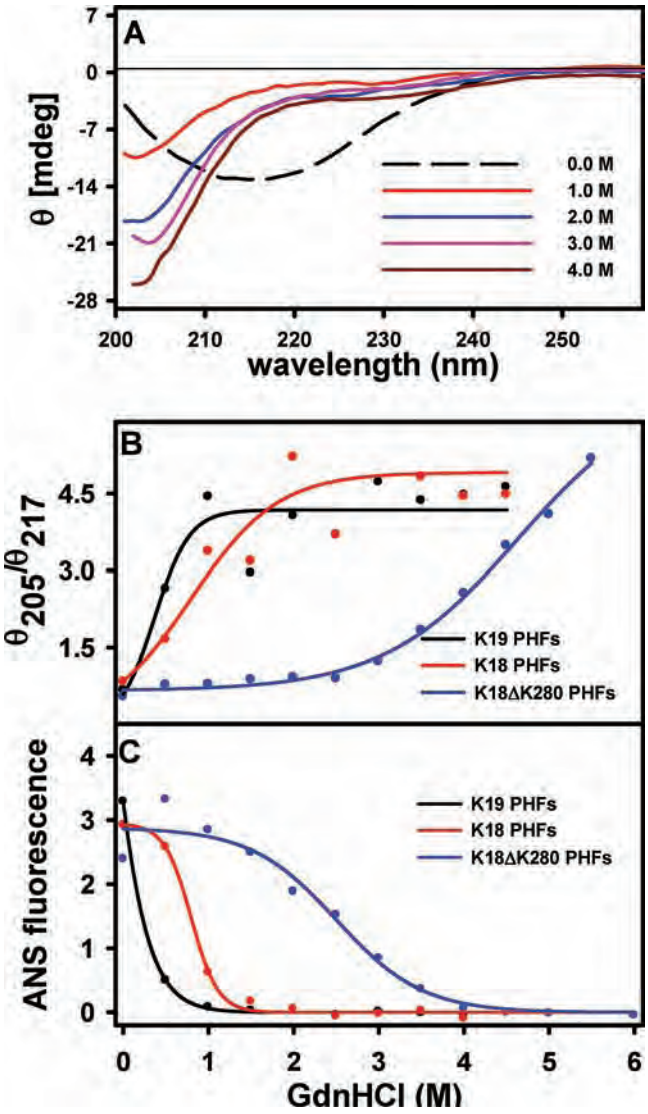

FIGURE 6: Denaturation of PHFs by GdnHCl. (A) CD spectra of K19-PHFs vs GdnHCl. PHFs were first assembled in standard conditions (20 mM BES pH 7.4 in the presence of heparin 6000; molar ratio of Tau:heparin = 4:1; incubation at 37 °C) and then treated with different concentrations of GdnHCl for 60 min at 20 °C. Without GdnHCl, the CD spectrum of PHFs shows a broad minimum around 217 nm reflecting the high β-sheet content. Already at 1 M GdnHCl, the β-structure is largely destroyed, and the spectrum changes toward that typical of denatured proteins. The spectra were taken with a 0.01 cm cuvette at 20 °C. (B) 205/217 nm ratio from GdnHCl denaturation of PHFs measured by CD. Note that the midpoint of the denaturation curve occurs at surprisingly low concentrations of GdnHCl, ~0.5 M for K19-PHFs and ~1 M for K18-PHFs confirming low stability of PHFs. By contrast, K18ΔK280-PHFs are much more resistant (midpoint ~4 M). (C) ANS fluorescence of PHFs against increasing GdnHCl. The ANS fluorescence decreases as the PHFs become denatured. The midpoints are comparable but lie at somewhat lower concentrations of GdnHCl, indicating that the hydrophobic pockets containing the bound ANS are destroyed faster than the overall β-structure.

a model of PHF dissolution where first the hydrophobic patches disappear before the secondary structure vanishes.

2. PHFs Are Sensitive to High or Low pH but Can Be Stabilized by Strong β-Structure. We next investigated the sensitivity of preformed PHFs to pH in the range 2−12 by CD. Preformed PHFs were incubated in buffer with different pH values for ~1 h at room temperature and then investigated by CD. K19-PHF samples showed partial β-structure at pH 7, but at pH 2 and 12 it showed a structural change toward a random coil (Figure 7A). A plot of the 200/217 nm ratio against pH revealed that K19-PHFs and K18-PHFs were stable between pH 6 and 9 but were gradually disrupted beyond this range, so that the β-structure of the PHFs visible around pH 7 converted to the random coil nature of the disassembled subunits at extreme pH values (pH 2 and 12) (Figure 7B). This suggests that the charged amino acids in the repeat domain play an important role in stabilizing PHFs via their ability to form ionic interactions. (Note: This partial disruption might also result from electrostatic repulsions at extreme pH values due to similar charges. But the core of K19-PHFs (I268−K343) contains only 5 acidic amino acids (2D + 3E) and 9 basic amino acids (9K) plus 3 histidine residues. Thus, disruption of K19-PHFs at both pH 2 and 12 indicates that it is not due to charge repulsion alone. If charge repulsion were the cause, disruption would be expected only at pH 2 since 12 amino acids are positively charged). This is supported by the recent analysis of K19-PHFs by solid state NMR indicating salt bridges within the PHF core (*1*). However, incubation at extreme pH values did not result in complete transition of PHFs to monomeric units as we found that the filaments incubated at pH 2 and 12 were shorter and thinner than those obtained at pH 7 in EM (Figure 7C), suggesting that they are fragmented during incubation or are more fragile and break easily during the preparation for EM. By contrast, K18ΔK280-PHFs showed no structural variation at any pH (Figure 7B). This argues that the increase in β-propensity in R2 can stabilize the PHF structure and overcompensate the loss of salt bridges.

3. Assembled PHFs Are Remarkably Resistant against Heat. The effect of temperature on preformed PHFs was analyzed during a temperature scan in the CD cell (5−95 °C, temperature rise 1 °C/min; Figure 8A,B). During this treatment, K19-PHFs retained their partial β-structure up to the highest temperature. After the temperature CD scan, PHFs were immediately brought to 25 °C and checked by ThS fluorescence, EM and SDS−PAGE. EM analysis showed that the morphology of filaments before and after the temperature-CD scan remained similar, suggesting that filaments are remarkably heat resistant (Figure S3A in the Supporting Information). However, the heat treatment caused about 40−50% disassembly of the PHFs, as judged by the loss of ThS fluorescence (Figure S3B in the Supporting Information) and pelleting assay (data not shown). In contrast, when PHFs were directly exposed to 95 °C for an hour and analyzed by pelleting assay, it showed no partial disaggregation (Figure S3C in the Supporting Information). Thus, the Tau aggregates showed a somewhat variable stability depending on whether they were treated by a stepwise rise of temperature (CD-temperature scan) or by direct exposure to high temperature. The partial dissociation of PHFs during the slow rise in temperature might reflect a partial stepwise dissolution of aggregates whereas a T-jump would be more prone to unspecific interactions. Thus, the thermal stability of preformed PHFs suggests a thermally resistant conformation of Tau filaments, possibly enabled by increased stability of directed salt bridges and strengthening of hydrophobic interactions between Tau molecules in PHFs. The unusual resistance of preassembled PHFs against heat treatment contrasts strongly with the heat sensitivity of de novo PHF formation (Figure 5B), suggesting that the heparin:

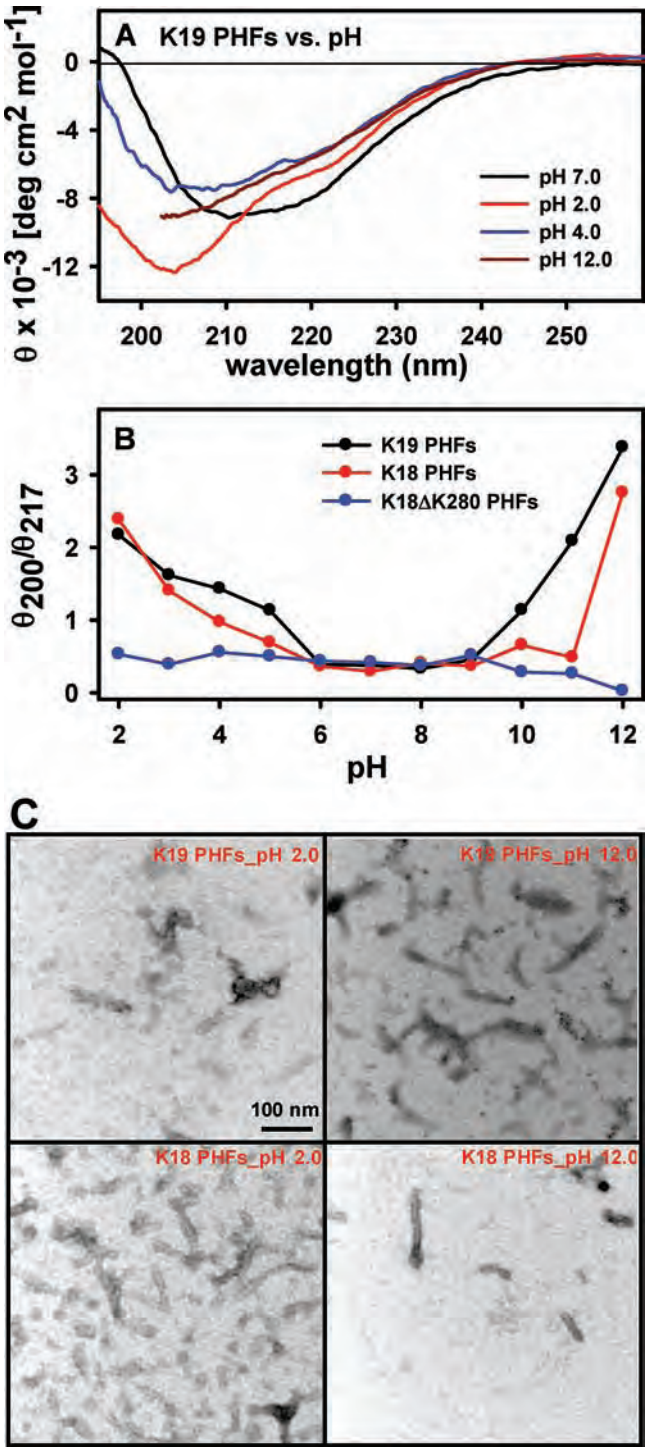

FIGURE 7: pH dependent structural transition of PHFs. (A) CD spectra of K19-PHFs at different pH values. Preformed Tau filaments (in 20 mM BES pH 7.4; heparin 6000; molar ratio of Tau:heparin = 4:1; incubation at 37 °C) were incubated at different pH values for 60 min at 20 °C and measured by CD. (B) 200/217 nm ratio from pH-dependent disaggregation of PHFs from K19, K18 and K18ΔK280 measured by CD. Note that PHFs from K18 or K19 begin to disintegrate above pH 9 or below pH 5, while K18ΔK280-PHFs are stable through most of the pH range. Secondary structure analysis (*65*) indicates that the random coil content of K19-PHF samples increases from pH 7 to pH 2 (from 38% to 53%), due to the partial disassembly of PHFs into subunits. Experimental conditions as in Figure 2. (C) Negative stain electron micrographs of K19 and K18 filaments after exposure to different pH values. Scale bar = 100 nm for all panels.

Tau interaction or the nucleating oligomeric intermediates are more easily disrupted by temperature.

4. PHFs Are Largely Resistant against Changes in Ionic Strength or Solvent Polarity. As in the case of high temperature, preassembled PHFs are also rather resistant to other changes in solvent conditions. Thus, an attempt to perturb the structure of PHFs at high salt concentrations (up to 750 mM Na_2SO_4) did not result in any change (Figure 8C,D). In view of the likely contribution of salt bridges to PHF structure, this result suggests that the core of PHFs is well protected from the solvent, consistent with other structural observations (*1*, *24*). The structure of the Tau filaments also remained largely unchanged when the solvent polarity was changed by isopropanol concentrations (5−25%, Figure 8E,F). The effect of alcohol on the stability of other amyloid fibrils reveals that either it completely dissolves (as in case of transthyretin$_{10-19}$ fibrils vs TFE) or it incompletely dissociates and leads to formation of other amorphous aggregates (as in the case of β2-microglobulin fibrils vs HFIP, TFE) (*39*, *40*).

DISCUSSION

Tau has drawn much interest because of its role in stabilizing microtubules for neurite outgrowth and axonal transport and for its pathological aggregation in Alzheimer disease. Structural studies on Tau indicate lack of defined structure (*41*, *42*). NMR spectroscopy confirms the paucity of secondary structure, but in addition highlights certain sequence motifs in the repeat domain with an enhanced propensity for β-structure which are known to play a role in the abnormal aggregation into PHFs (*4*−*6*, *8*). Although there are differences in interpretation on structural elements in other regions, e.g. random coil vs short α-helix (*6*, *8*), there is consensus on the β-structure in the nucleating hexapeptide motifs. We have investigated the structural variation of soluble Tau and its aggregation into filaments in order to understand the unfolded character of the protein and factors contributing to its aggregation.

1. Low Hydrophobicity Defines Unfolded Nature of Soluble Tau. A high net charge and low hydrophobicity are held responsible for the unfolded nature of proteins (*9*). We tested these parameters on Tau by monitoring structural transitions by CD under changing solvent conditions. A change of pH did not alter the secondary structure of full-length Tau (hTau40wt) or its repeat-domain constructs (K19, K18 and K18ΔK280). Even though the charge of the repeat domain (net charges ∼+9) is neutralized around pH 10, it failed to undergo a structural transition toward a collapsed state, consistent with the low content of hydrophobic amino acids that can drive folding upon charge neutralization. In the case of full-length Tau, the assumption that a high net charge is a requirement for unfoldedness does not apply. The net charge is only +2, yet this protein remains unfolded in all solvent conditions. This unusual behavior can be explained by the multidomain nature of Tau, which is effectively a combination of several domains, each of which has a high net charge. By contrast, α-synuclein (pI = 4.44) undergoes a well-defined structural transition between pH 2 and 8 (*23*), consistent with the presence of the central NAC domain that is abundant in hydrophobic amino acids. On the other hand, securin (pI = 6.2), another natively unfolded protein, also

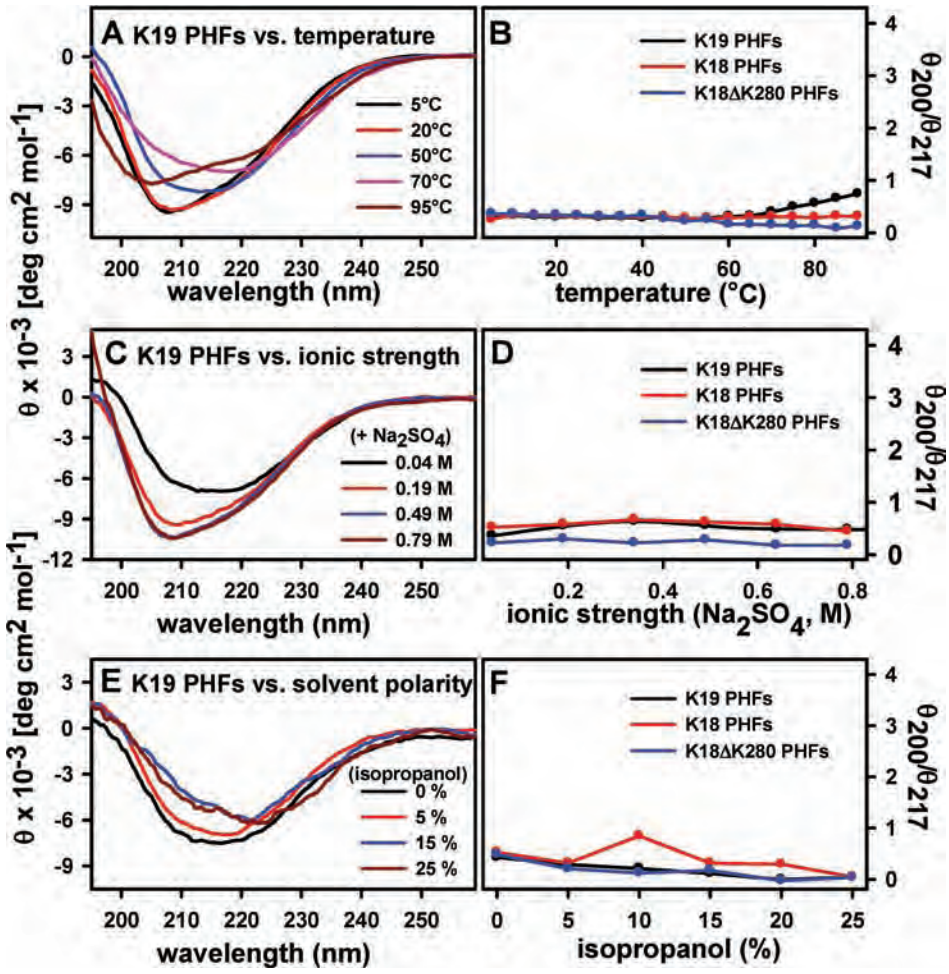

FIGURE 8: Structure of PHFs at elevated temperature, in high ionic strength and changing solvent polarity. Preformed Tau filaments (20 mM BES pH 7.4; heparin 6000; molar ratio of Tau:heparin = 4:1; incubation at 37 °C) were analyzed in CD upon temperature elevation, in high ionic strength and changing solvent polarity. (A and B) CD spectra of K19-PHFs and 200/217 nm ratio at different temperatures. Spectra were measured continuously with 1 °C/min from 5 to 95 °C. The structure of PHFs largely unaffected at elevated temperatures, probably due to the contribution of increased hydrophobic interactions and directed salt bridges. (C and D) CD spectra of K19-PHFs and 200/217 nm ratio at various salt concentrations. (E and F) CD spectra of K19-PHFs and 200/217 nm ratio at varying isopropanol concentration. Note that the structure of PHFs is largely unaltered by high salt and isopropanol concentration. Experimental conditions as in Figure 2.

shows an unaltered structure as a function of pH (*25*), similar to the behavior of Tau upon pH variation. It is interesting to note that securin also exhibit multidomain nature similar to Tau by having basic N-terminus and acidic C-terminus.

The temperature-dependent CD spectra of Tau suggest a small and gradual change that can be explained by a transition between two states, indicated by the isobestic point at 210 nm. However, unlike globular proteins (e.g., lysozyme, cytochrome *c*), there is no cooperative transition. This illustrates the lack of significant hydrophobicity to drive a hydrophobic collapse. The characteristics of temperature-dependent CD spectra of PPII peptides are similar to those observed here for Tau. In the case of PPII peptides, the spectral change upon temperature rise is attributed to the transition from a mostly PPII structure to a more disordered or extended structure (*27*). Judging by NMR and Raman optical activity, Tau contains little PPII helix in the strict sense (*7, 43*), whereas random coil and partially extended structure is pronounced on the background of a highly flexible structure throughout (*6, 7*). Based on these observations, it is reasonable to assume that Tau has an appreciable contribution from PPII structure at low temperature, which becomes randomized and more extended at high temperature. Nevertheless, in the case of PPII there is a debate on the correspondence between values derived from CD and NMR. The conformational ensembles of an unfolded protein are highly heterogeneous. Hence, any interpretation from a single spectroscopic parameter reflects the qualitative nature of these average structures which are highly ensemble and position dependent. In the cases of α-synuclein and securin, one observes a similar filling-in of the CD-trough at 200 nm, however, the interpretations vary: formation of a partially folded intermediate due to the increase of hydrophobic interactions in case of α-synuclein (*23*) vs PPII structure in the case of securin (*25*). Apart from that, the inability of salt to induce folding in soluble Tau reinforces the notion that the unfoldedness of Tau is mainly due to the low content of hydrophobic amino acids. Changing the solvent polarity by moderate concentrations of isopropanol induces a slight effect on the structure of Tau, but most of the random coil signature of Tau remains even at 25% alcohol.

The physiological implication of the persistent unfolded nature of Tau even upon variation in pH, high salt or solvent polarity is that the conformation likely remains unchanged even upon binding to microtubules. Charge neutralization or shielding of charged amino acids upon pH variation and

salt could have a similar effect as the interaction of the basic amino acids of the Tau repeat domain with the acidic C-terminal tail of tubulin subunits. In support of this view, EM studies showed that Tau retains much of its unfolded nature even in the presence of microtubules (*12, 13*). However, it is quite possible that Tau changes some conformations when it binds to microtubules, and that it "freezes in" some conformations, at least in the microtubule-binding domain of Tau, analogous to adopted loop structure with no intrachain hydrogen bonds of Tau peptide (T386−E391) upon binding to MN423 antibody (*44*). Besides, there is the possibility of formation of short α-helical segments on negatively charged binding surfaces, as detected by NMR (*45*), which would not be detectable in the global CD pattern.

2. Optimization of Aggregation of Tau. Since conditions for Tau aggregation vary between different studies, we tested aggregation for the cases of Tau constructs K19 and K18 over a wide range. The aggregation of Tau was found to be enhanced upon (i) charge neutralization at pH values near but below p*I*, (ii) optimal temperature (∼50 °C), (iii) low salt concentration. For K19 and K18 the efficiency of aggregation is low at pH < 5; moderate between pH 6 and 7 and high between pH 8−10, just below the p*I* (∼10.4). The enhanced aggregation at pH 8−10 can be explained by the minimization of the net charge of Tau constructs (Figure 1A), thus facilitating the neutralization of the remaining charges by heparin. Concomitant with the low net charge at high pH, the interaction between the known hydrophobic patches of Tau molecules could be favored in the presence of heparin. Heparin as a cofactor for aggregation appears to be necessary in all conditions, since Tau alone failed to aggregate even at pH values just below the p*I* where the charge is minimized. Thus, heparin may specifically act by shielding certain basic amino acids involved in the nucleation of aggregation. For example, lysine ($pK_a = 10.53$) is still partially charged at pH 10 but loses the charge at higher pH. Such lysine residues (e.g., K312 in PHF6 and K331) are reported to interact with heparin as well as microtubules (*6*). At pH < 4 or > 11, the protonation or deprotonation of charged amino acids would result in the inability to form salt bridges. It is also expected that low pH values would affect the charged sites of heparin resulting in the failure of heparin to bind to Tau.

Increasing the salt concentration strongly attenuated the aggregation. The salt can affect interactions of protein side chains and backbone with the solvent water, thus shielding charged residues. There is a debate on whether heparin promotes Tau aggregation only during nucleation or whether it is incorporated into PHFs (*46*−*48*), but in either case the two components are expected to interact electrostatically, based on the formation of new salt bridges during aggregation. Thus the salt-dependent inhibition of aggregation would be explained by the disruption of electrostatic interactions (heparin−Tau or Tau−Tau) (*30*). The aggregation of Tau showed an optimal temperature of 50 °C and decreased at higher temperatures (>60 °C). Given the highly charged nature of Tau, the temperature dependence of aggregation is likely dominated by specific ionic interactions along with hydrophobic interactions, both of which have the same temperature dependence (*34, 49*). This points to fact that Tau aggregation up to 50 °C should be partially entropy-driven, since the loss of interactions of monomeric protein with solvent water at high temperature is compensated by the interactions between them. At temperatures higher than 50 °C, the decrease in aggregation can be explained by the increase of kinetic energy that overcomes the cohesion of directed salt bridges and hydrophobic interactions between Tau molecules and between Tau and heparin. This would be consistent with the failure of nucleation events at high temperature which are necessary for filament formation.

Tau aggregation monitored by the environment sensitive fluorophore ANS suggested the formation of hydrophobic pockets in PHFs. ANS is widely used to detect solvent-exposed hydrophobic clusters in proteins and protein aggregates. The primary sequence of Tau has low hydrophobic content but contains two known hydrophobic stretches at the beginning of R2 and R3. Hence, the increased ANS fluorescence as Tau polymerized is likely to arise from a direct interaction of the PHF6 and PHF6* motifs of two Tau molecules during β-sheet formation upon aggregation. In fact, the ANS fluorescence of assembling K18 (containing two hydrophobic hexapeptides) showed higher values than K19 (having only one hexapeptide motif). The binding of ANS to partially folded intermediate of Tau in the presence of arachidonic acid, that precedes aggregation, has also been reported earlier (*50*). However, tryptophan quenching experiments showed that the core of Tau filaments is rather inaccessible (*24*). This observation opposes a view that ANS would bind to the hexapaptide motifs inside the core. In fact, the binding mechanism of fluorescent dyes such as ThS, ANS and others to amyloid aggregates is poorly understood and a matter of debate (*51, 52*). It is worth noting that the structure of the bacterial protein MurA in complex with ANS revealed that the naphthalene ring of ANS is sandwiched between a Pro and the hydrophobic side chain of Arg where the sulfonate group is hydrogen-bonded to the main-chain amide of Gly and to the guanidinium group of Arg (*53*). The distance between the center of the ANS molecule and the carbon atoms of the protein is ∼3.5 Å on both sides. This distance is very close to the distance between the side chains of two amino acids in cross β-structure. Thus, it is possible that ANS binds to the accessible surface of the PHF core where it can intercalate between the side chains of amino acids that are facing outside. This would be consistent with a recent model of the PHF core derived from solid state NMR experiments (*1*).

3. The Stability of PHFs Depends on Salt Bridges. Tau filaments are built on a cross β-structure that is typical for amyloid aggregates (*54*). However, the factors contributing to the stability can vary considerably. The present study used PHFs derived from repeat domain constructs for analyzing stability. This is based on several experimental approaches (e.g., resistance against digestion by proteases, fluorescence quenching, NMR) that agree that the repeat domain includes the core of PHFs (*24, 47, 55, 56*). Our analysis of the stability of preformed PHFs is as follows: (i) PHFs have a mild denaturation transition point (∼1.0 M GdnHCl), much lower than that required to denature a globular protein like tubulin (∼4.5 M GdnHCl), indicating a small contribution of hydrophobic interactions for the stability. In contrast, PHFs made from the FDTP17 mutant K18ΔK280 show a much higher stability and faster assembly kinetics that is explained by the formation of a larger amphipathic patch at the nucleating hexapeptide motif PHF6* (*4*). (ii) A partial

disruption of PHFs at extreme pH values was observed by CD and EM. This reinforces the importance of salt bridges for the stability of PHFs because the protonation of aspartic and glutamatic acid residues at pH < 4 and deprotonation of lysine and arginine at pH > 10 could disturb the ionic interaction between them. The structure of K18ΔK280-PHFs remained unchanged even at extreme pH values, corresponding to a tighter interaction of the enlarged hydrophobic patches caused by the longer β-strand in the PHF6* motif (*4*). (iii) PHFs composed of Tau, a highly soluble protein with only small hydrophobic patches compared to other amyloidogenic proteins such as Aβ(1−42) and β2-microglobulin, show resistance to high temperature. The thermal stability of PHFs indicates that they are held together by specific ionic interactions and hydrophobic interactions that are favored at high temperatures (*34*, *49*). Fibrils of Aβ(1−42) and β2-microglobulin exhibit partial dissociation from 60 °C onward, but complete dissociation is possible above 100 °C (*57*). In general, the thermal stability of amyloid fibrils might not be surprising. For example, heating of hen eggs and wool fibers is known to cause irreversible aggregation with transformation of α-helix patterns to cross-β patterns (*58*). The thermal stability of fibrils can be explained by the structural organization of fibrils such as a specific arrangement of the hydrophobic and hydrogen-bonding residues (*54*, *59*). On other hand, since most of the amyloidogenic proteins can aggregate at high temperature, the thermal stability of fibrils may depend on the equilibrium between the dissociation of monomers and their aggregation (to amyloid fibrils or other amorphous aggregates). (iv) PHFs are undisturbed at high salt and moderate isopropanol concentrations, reinforcing the notion that once PHFs are formed, the molecular interactions are rather stable.

A few studies on the stability of other amyloid aggregates also support the contribution of salt bridges and hydrophobic interactions. The high resolution structure of amyloid fiber from peptide KFFEAAAKKFFE showed that fibers consist of antiparallel β-sheets that are zippered together by means of π-bonding between adjacent phenylalanine rings and salt-bridges between charge pairs (glutamic acid−lysine), thus controlling and stabilizing the structure (*60*). Likewise, the major contribution of ionic interactions with minor hydrophobic interactions to stability of PHFs (depicted in Figure 9) is supported by some previous studies on Tau filaments. The importance of charged amino acids for Tau aggregation was recently shown where the deletion of K311 (in hexapeptide motif PHF6) was found to abolish polymerization, leading to the speculation that this lysine residue is involved in the formation of salt bridge (*61*). Crystals obtained from the hexapeptide PHF6 (VQIVYK) have been solved by X-ray crystallography and show a cross β-spine structure, arranged in a zipperlike fashion forming a dry interface (dominated by hydrophobic interactions) and a wet interface (dominated by ionic interactions) (*54*). A similar model of filaments from Tau protein might support the disturbance of a wet interface upon pH variation due to the loss of ionic interactions. By contrast, the β-helix model proposed on the basis of an EPR analysis of hTau40 does not directly reveal the role of ionic interactions (*62*). However, it cannot be ruled out that there are ionic interactions between oppositely charged amino acids or between Tau and residual heparin that interacts along the fiber axis. (Note: Since only minimal content of heparin is shown to be incorporated into PHFs (*46*, *47*), the subunit interactions within PHFs would be mainly as Tau−Tau interactions. However, there is also hypothesis that heparin is incorporated into PHFs (*48*).) Recent studies based on solid state NMR of K19-PHFs emphasized the importance of salt bridges in the PHF core (*1*). Finally, the difference in stability between PHFs from AD brains and PHFs assembled in vitro is not a fundamental one as both have similar protease-resistant core and show a supertwist repeat of about 80 nm. In addition, as filaments assembled in vitro are labile, the incipient formation of PHFs is reversible, as shown by recent cell and mouse models of Tauopathy (*63*, *64*). Thus, the results from the present study could form a basis for elucidating the molecular architecture of PHFs.

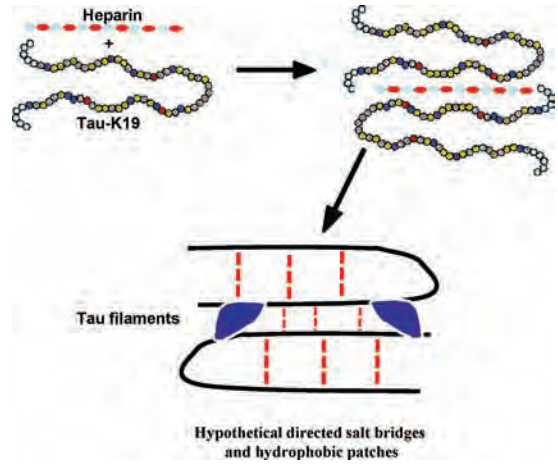

FIGURE 9: Model of PHF stabilizing factors. Soluble Tau upon incubation dimerizes and in the presence of heparin aggregates into PHFs. Heparin is believed to neutralize the charge in the basic repeat region of Tau, thus enhancing aggregation. Upon aggregation, Tau shows an increase of hydrophobic patches probably due to direct interaction of known β-structural elements of Tau in R3 and R2 (PHF6 and PHF6* respectively). The preformed PHFs are labile as evidenced by the low denaturation point (corresponding to the absence of major contributions from hydrophobic interactions) and partial disruption at extreme pH values (corresponding to major contribution from salt bridges, in agreement with the recent model of the PHF core (*1*). The repulsion of similarly charged residues would also contribute to the disruption of PHFs but would be expected only at an extreme pH value due to large number of basic amino acids compared to acidic amino acids within the core of PHFs. Thus once PHFs are formed, salt bridges are likely the major stabilizing elements of PHFs, with minor contributions from hydrophobic pockets.

ACKNOWLEDGMENT

We would like to thank Bianca Scharnweber for excellent technical assistance. We also thank Dr. Jacek Biernat for Tau constructs, Dr. Alexander Marx for useful discussions and Dr. Marcus Pickhardt for help with electron microscopy.

SUPPORTING INFORMATION AVAILABLE

Figure S1 shows the aggregation efficiency of the 4-repeat Tau construct K18 at different pH values and EM pictures of K18 filaments (analogous to the data of Figure 4 in the main text for construct K19). Figure S2 shows the aggregation efficiency of K18 vs increasing ionic strength and elevated temperature, as well as the aggregation of full length isoform hTau40 monitored by the fluorescence of ANS and ThS (analogous to the data of Figure 5 in the main text for

construct K19). Figure S3 shows EM pictures of filaments of K19 and K18 before and after a temperature scan and the corresponding pelleting assay (corresponding to the data of Figure 8). This material is available free of charge via the Internet at http://pubs.acs.org.

REFERENCES

1. Andronesi, O. C., von Bergen, M., Biernat, J., Seidel, K., Griesinger, C., Mandelkow, E., and Baldus, M. (2008) Characterization of Alzheimer's-like paired helical filaments from the core domain of tau protein using solid-state NMR spectroscopy. *J. Am. Chem. Soc. 130*, 5922–5928.
2. Garcia, M. L., and Cleveland, D. W. (2001) Going new places using an old MAP: tau, microtubules and human neurodegenerative disease. *Curr. Opin. Cell Biol. 13*, 41–48.
3. Mandelkow, E., von Bergen, M., Biernat, J., and Mandelkow, E. M. (2007) Structural principles of tau and the paired helical filaments of Alzheimer's disease. *Brain Pathol. 17*, 83–90.
4. von Bergen, M., Barghorn, S., Li, L., Marx, A., Biernat, J., Mandelkow, E. M., and Mandelkow, E. (2001) Mutations of tau protein in frontotemporal dementia promote aggregation of paired helical filaments by enhancing local beta-structure. *J. Biol. Chem. 276*, 48165–48174.
5. von Bergen, M., Friedhoff, P., Biernat, J., Heberle, J., Mandelkow, E. M., and Mandelkow, E. (2000) Assembly of tau protein into Alzheimer paired helical filaments depends on a local sequence motif ((306)VQIVYK(311)) forming beta structure. *Proc. Natl. Acad. Sci. U.S.A. 97*, 5129–5134.
6. Mukrasch, M. D., Biernat, J., von Bergen, M., Griesinger, C., Mandelkow, E., and Zweckstetter, M. (2005) Sites of tau important for aggregation populate {beta}-structure and bind to microtubules and polyanions. *J. Biol. Chem. 280*, 24978–24986.
7. Mukrasch, M. D., von Bergen, M., Biernat, J., Fischer, D., Griesinger, C., Mandelkow, E., and Zweckstetter, M. (2007) The "jaws" of the tau-microtubule interaction. *J. Biol. Chem. 282*, 12230–12239.
8. Eliezer, D., Barre, P., Kobaslija, M., Chan, D., Li, X., and Heend, L. (2005) Residual structure in the repeat domain of tau: echoes of microtubule binding and paired helical filament formation. *Biochemistry 44*, 1026–1036.
9. Uversky, V. N. (2002) What does it mean to be natively unfolded? *Eur. J. Biochem. 269*, 2–12.
10. Uversky, V. N., Oldfield, C. J., and Dunker, A. K. (2005) Showing your ID: intrinsic disorder as an ID for recognition, regulation and cell signaling. *J. Mol. Recognit. 18*, 343–384.
11. Butner, K. A., and Kirschner, M. W. (1991) Tau protein binds to microtubules through a flexible array of distributed weak sites. *J. Cell Biol. 115*, 717–730.
12. Santarella, R. A., Skiniotis, G., Goldie, K. N., Tittmann, P., Gross, H., Mandelkow, E. M., Mandelkow, E., and Hoenger, A. (2004) Surface-decoration of microtubules by human tau. *J. Mol. Biol. 339*, 539–553.
13. Al-Bassam, J., Ozer, R. S., Safer, D., Halpain, S., and Milligan, R. A. (2002) MAP2 and tau bind longitudinally along the outer ridges of microtubule protofilaments. *J. Cell Biol. 157*, 1187–1196.
14. Woody, R. W., Clark, D. C., Roberts, G. C., Martin, S. R., and Bayley, P. M. (1983) Molecular flexibility in microtubule proteins: proton nuclear magnetic resonance characterization. *Biochemistry 22*, 2186–2192.
15. Sillen, A., Barbier, P., Landrieu, I., Lefebvre, S., Wieruszeski, J. M., Leroy, A., Peyrot, V., and Lippens, G. (2007) NMR Investigation of the Interaction between the Neuronal Protein Tau and the Microtubules. *Biochemistry 46*, 3055–3064.
16. Goedert, M., Jakes, R., Spillantini, M. G., Hasegawa, M., Smith, M. J., and Crowther, R. A. (1996) Assembly of microtubule-associated protein tau into Alzheimer-like filaments induced by sulphated glycosaminoglycans. *Nature 383*, 550–553.
17. Schweers, O., Mandelkow, E. M., Biernat, J., and Mandelkow, E. (1995) Oxidation of cysteine-322 in the repeat domain of microtubule-associated protein tau controls the in vitro assembly of paired helical filaments. *Proc. Natl. Acad. Sci. U.S.A. 92*, 8463–8467.
18. Wilson, D. M., and Binder, L. I. (1997) Free fatty acids stimulate the polymerization of tau and amyloid beta peptides. In vitro evidence for a common effector of pathogenesis in Alzheimer's disease. *Am. J. Pathol. 150*, 2181–2195.
19. Chirita, C. N., Necula, M., and Kuret, J. (2003) Anionic micelles and vesicles induce tau fibrillization in vitro. *J. Biol. Chem. 278*, 25644–25650.
20. Barghorn, S., Biernat, J., and Mandelkow, E. (2005) Purification of recombinant tau protein and preparation of Alzheimer-paired helical filaments in vitro. *Methods Mol. Biol. 299*, 35–51.
21. Rice, P., Longden, I., and Bleasby, A. (2000) EMBOSS: the European Molecular Biology Open Software Suite. *Trends Genet. 16*, 276–277.
22. Prilusky, J., Felder, C. E., Zeev-Ben-Mordehai, T., Rydberg, E. H., Man, O., Beckmann, J. S., Silman, I., and Sussman, J. L. (2005) FoldIndex: a simple tool to predict whether a given protein sequence is intrinsically unfolded. *Bioinformatics 21*, 3435–3438.
23. Uversky, V. N., Li, J., and Fink, A. L. (2001) Evidence for a partially folded intermediate in alpha-synuclein fibril formation. *J. Biol. Chem. 276*, 10737–10744.
24. Li, L., von Bergen, M., Mandelkow, E. M., and Mandelkow, E. (2002) Structure, stability, and aggregation of paired helical filaments from tau protein and FTDP-17 mutants probed by tryptophan scanning mutagenesis. *J. Biol. Chem. 277*, 41390–41400.
25. Sanchez-Puig, N., Veprintsev, D. B., and Fersht, A. R. (2005) Human full-length Securin is a natively unfolded protein. *Protein Sci. 14*, 1410–1418.
26. Dill, K. A., Fiebig, K. M., and Chan, H. S. (1993) Cooperativity in protein-folding kinetics. *Proc. Natl. Acad. Sci. U.S.A. 90*, 1942–1946.
27. Eker, F., Griebenow, K., and Schweitzer-Stenner, R. (2003) Stable conformations of tripeptides in aqueous solution studied by UV circular dichroism spectroscopy. *J. Am. Chem. Soc. 125*, 8178–8185.
28. Shiraki, K., Nishikawa, K., and Goto, Y. (1995) Trifluoroethanol-induced stabilization of the α-helical structure of beta-lactoglobulin: implication for non-hierarchical protein folding. *J. Mol. Biol. 245*, 180–194.
29. Chiti, F., and Dobson, C. M. (2006) Protein misfolding, functional amyloid, and human disease. *Annu. Rev. Biochem. 75*, 333–366.
30. Friedhoff, P., Schneider, A., Mandelkow, E. M., and Mandelkow, E. (1998) Rapid assembly of Alzheimer-like paired helical filaments from microtubule-associated protein tau monitored by fluorescence in solution. *Biochemistry 37*, 10223–10230.
31. Congdon, E. E., Kim, S., Bonchak, J., Songrug, T., Matzavinos, A., and Kuret, J. (2008) Nucleation-dependent tau filament formation: the importance of dimerization and an estimation of elementary rate constants. *J. Biol. Chem. 283*, 13806–13816.
32. Munishkina, L. A., Henriques, J., Uversky, V. N., and Fink, A. L. (2004) Role of protein-water interactions and electrostatics in alpha-synuclein fibril formation. *Biochemistry 43*, 3289–3300.
33. Raman, B., Chatani, E., Kihara, M., Ban, T., Sakai, M., Hasegawa, K., Naiki, H., Rao Ch, M., and Goto, Y. (2005) Critical balance of electrostatic and hydrophobic interactions is required for beta 2-microglobulin amyloid fibril growth and stability. *Biochemistry 44*, 1288–1299.
34. Elcock, A. H. (1998) The stability of salt bridges at high temperatures: implications for hyperthermophilic proteins. *J. Mol. Biol. 284*, 489–502.
35. Arora, A., Ha, C., and Park, C. B. (2004) Insulin amyloid fibrillation at above 100 degrees C: new insights into protein folding under extreme temperatures. *Protein Sci. 13*, 2429–2436.
36. Semisotnov, G. V., Rodionova, N. A., Razgulyaev, O. I., Uversky, V. N., Gripas, A. F., and Gilmanshin, R. I. (1991) Study of the "molten globule" intermediate state in protein folding by a hydrophobic fluorescent probe. *Biopolymers 31*, 119–128.
37. Nozaki, Y., and Tanford, C. (1970) The solubility of amino acids, diglycine, and triglycine in aqueous guanidine hydrochloride solutions. *J. Biol. Chem. 245*, 1648–1652.
38. Schellman, J. A. (1987) Selective binding and solvent denaturation. *Biopolymers 26*, 549–559.
39. MacPhee, C. E., and Dobson, C. M. (2000) Chemical dissection and reassembly of amyloid fibrils formed by a peptide fragment of transthyretin. *J. Mol. Biol. 297*, 1203–1215.
40. Hirota-Nakaoka, N., Hasegawa, K., Naiki, H., and Goto, Y. (2003) Dissolution of beta2-microglobulin amyloid fibrils by dimethylsulfoxide. *J. Biochem. 134*, 159–164.
41. Cleveland, D. W., Hwo, S. Y., and Kirschner, M. W. (1977) Physical and chemical properties of purified tau factor and the role of tau in microtubule assembly. *J. Mol. Biol. 116*, 227–247.
42. Schweers, O., Schonbrunn-Hanebeck, E., Marx, A., and Mandelkow, E. (1994) Structural studies of tau protein and Alzheimer

paired helical filaments show no evidence for beta-structure. *J. Biol. Chem. 269*, 24290–24297.
43. Syme, C. D., Blanch, E. W., Holt, C., Jakes, R., Goedert, M., Hecht, L., and Barron, L. D. (2002) A Raman optical activity study of rheomorphism in caseins, synucleins and tau. New insight into the structure and behaviour of natively unfolded proteins. *Eur. J. Biochem. 269*, 148–156.
44. Sevcik, J., Skrabana, R., Dvorsky, R., Csokova, N., Iqbal, K., and Novak, M. (2007) X-ray structure of the PHF core C-terminus: insight into the folding of the intrinsically disordered protein tau in Alzheimer's disease. *FEBS Lett. 581*, 5872–5878.
45. Barre, P., and Eliezer, D. (2006) Folding of the repeat domain of tau upon binding to lipid surfaces. *J. Mol. Biol. 362*, 312–326.
46. Carlson, S. W., Branden, M., Voss, K., Sun, Q., Rankin, C. A., and Gamblin, T. C. (2007) A complex mechanism for inducer mediated tau polymerization. *Biochemistry 46*, 8838–8849.
47. von Bergen, M., Barghorn, S., Muller, S. A., Pickhardt, M., Biernat, J., Mandelkow, E. M., Davies, P., Aebi, U., and Mandelkow, E. (2006) The core of tau-paired helical filaments studied by scanning transmission electron microscopy and limited proteolysis. *Biochemistry 45*, 6446–6457.
48. Sibille, N., Sillen, A., Leroy, A., Wieruszeski, J. M., Mulloy, B., Landrieu, I., and Lippens, G. (2006) Structural impact of heparin binding to full-length Tau as studied by NMR spectroscopy. *Biochemistry 45*, 12560–12572.
49. Baldwin, R. L. (1986) Temperature dependence of the hydrophobic interaction in protein folding. *Proc. Natl. Acad. Sci. U.S.A. 83*, 8069–8072.
50. Chirita, C. N., and Kuret, J. (2004) Evidence for an intermediate in tau filament formation. *Biochemistry 43*, 1704–1714.
51. LeVine, H. 3rd. (2005) Multiple ligand binding sites on A beta(1−40) fibrils. *Amyloid 12*, 5–14.
52. Inouye, H., and Kirschner, D. A. (2005) Alzheimer's beta-amyloid: insights into fibril formation and structure from Congo red binding. *Subcell. Biochem. 38*, 203–224.
53. Schonbrunn, E., Eschenburg, S., Luger, K., Kabsch, W., and Amrhein, N. (2000) Structural basis for the interaction of the fluorescence probe 8-anilino-1-naphthalene sulfonate (ANS) with the antibiotic target MurA. *Proc. Natl. Acad. Sci. U.S.A. 97*, 6345–6349.
54. Sawaya, M. R., Sambashivan, S., Nelson, R., Ivanova, M. I., Sievers, S. A., Apostol, M. I., Thompson, M. J., Balbirnie, M., Wiltzius, J. J., McFarlane, H. T., Madsen, A. O., Riekel, C., and Eisenberg, D. (2007) Atomic structures of amyloid cross-beta spines reveal varied steric zippers. *Nature 447*, 453–457.
55. Sillen, A., Leroy, A., Wieruszeski, J. M., Loyens, A., Beauvillain, J. C., Buee, L., Landrieu, I., and Lippens, G. (2005) Regions of tau implicated in the paired helical fragment core as defined by NMR. *ChemBioChem 6*, 1849–1856.
56. Wischik, C. M., Novak, M., Edwards, P. C., Klug, A., Tichelaar, W., and Crowther, R. A. (1988) Structural characterization of the core of the paired helical filament of Alzheimer disease. *Proc. Natl. Acad. Sci. U.S.A. 85*, 4884–4888.
57. Sasahara, K., Naiki, H., and Goto, Y. (2005) Kinetically controlled thermal response of beta2-microglobulin amyloid fibrils. *J. Mol. Biol. 352*, 700–711.
58. Astbury, W. T., and Dickinson, S. (1935) The X-ray interpretation of denaturation and the structure of the seed globulins. *Biochem. J. 29*, 2351–2360, 2351.
59. Meersman, F., and Dobson, C. M. (2006) Probing the pressure-temperature stability of amyloid fibrils provides new insights into their molecular properties. *Biochim. Biophys. Acta 1764*, 452–460.
60. Makin, O. S., Atkins, E., Sikorski, P., Johansson, J., and Serpell, L. C. (2005) Molecular basis for amyloid fibril formation and stability. *Proc. Natl. Acad. Sci. U.S.A. 102*, 315–320.
61. Li, W., and Lee, V. M. (2006) Characterization of Two VQIXXK Motifs for Tau Fibrillization in Vitro. *Biochemistry 45*, 15692–15701.
62. Margittai, M., and Langen, R. (2004) Template-assisted filament growth by parallel stacking of tau. *Proc. Natl. Acad. Sci. U.S.A. 101*, 10278–10283.
63. Khlistunova, I., Biernat, J., Wang, Y., Pickhardt, M., von Bergen, M., Gazova, Z., Mandelkow, E., and Mandelkow, E. M. (2006) Inducible expression of Tau repeat domain in cell models of tauopathy: aggregation is toxic to cells but can be reversed by inhibitor drugs. *J. Biol. Chem. 281*, 1205–1214.
64. Oddo, S., Billings, L., Kesslak, J. P., Cribbs, D. H., and LaFerla, F. M. (2004) Abeta immunotherapy leads to clearance of early, but not late, hyperphosphorylated tau aggregates via the proteasome. *Neuron 43*, 321–332.
65. Yang, J. T., Wu, C. S., and Martinez, H. M. (1986) Calculation of protein conformation from circular dichroism. *Methods Enzymol. 130*, 208–269.

BI800783D

The Natively Unfolded Character of Tau and its Aggregation to Alzheimer-like Paired Helical Filaments

Sadasivam Jeganathan[¶*], Martin von Bergen[#], Eva-Maria Mandelkow[¶], Eckhard Mandelkow[¶*]

SUPPLEMENTARY INFORMATION

Supplementary Figure 1: Aggregation efficiency of tau 4R construct-K18 in different buffers and pH, at high salt concentration and elevated temperatures. **(A)** Aggregation of K18 was induced with 50 µM K18 protein in 20 mM buffer of different compositions and pH values in the presence of heparin 3000 (molar ratio of tau:heparin = 4:1). The samples were incubated at 37°C for 3 days and the extent of aggregation was then measured by ThS fluorescence. Note that K18 aggregation is significantly better at pH values just below its isoelectric point. **(B)** The average fluorescence intensity of the assembly reaction in all buffers of each pH value. Note that tau aggregation requires the presence of heparin even at pH values that minimize the charge. **(C)** EM pictures of filaments of K18 obtained in different conditions of buffer and pH are shown. Scale bar = 100 nm for all images. In all cases, the extent of aggregation was measured by ThS fluorescence as described in Fig. 4.

Supplementary Figure 2: (A) Relative ThS fluorescence is shown from polymerization reactions of K18 at various salt concentrations. Note that aggregation is diminished as salt concentration is increased. **(B)** Relative ThS fluorescence is shown from polymerization reactions of K18 at various temperatures. Note that aggregation shows an optimum in the temperature dependence. In all cases, the extent of aggregation was measured by ThS fluorescence as described in Fig. 4. **(C) & (D)** Aggregation of htau40 monitored by the fluorescence of ANS & ThS. Aggregation was started with 50 µM protein in the presence of heparin 5000 (molar ratio of tau:heparin = 4:1) and incubated at 37°C. The aggregation monitored by ANS fluorescence (C) and ThS fluorescence (D). The measurement conditions are as

described in Fig 4 & Fig.5. Note that the increase of ANS and ThS fluorescence are equivalent as the aggregation proceeds, with ANS fluorescence lesser than for K18 or K19 confirming the formation of hydrophobic pockets are confined to repeat regions.

Supplementary Figure 3: Temperature resistant PHFs. (A) EM pictures of filaments of K19 and K18 before and after CD-temperature scan (1˚C/min, range 5-95˚C). Note that the morphology of filaments after the CD-temperature scan is similar to that of filaments before. **(B)** ThS fluorescence measurements from filaments before and after CD-temperature scan. PHFs after high temperature exposure showed a decrease in ThS fluorescence, indicating PHFs are partially dissociated. **(C)** SDS gel analysis of PHFs exposed to high salt, temperature jump and GdnHCl by pelleting assay. K19-PHFs and K18ΔK280-PHFs were incubated in 20 mM Na phosphate pH 7.0 buffer, in buffer + 759 mM Na_2SO_4 at 20˚C or incubated directly at 95˚C for ~ 1 hour (temperature jump), and treated with 3.2 M GdnHCl for 15 minutes at 20˚C. All the incubated samples were pelleted by centrifugation (16000 x g, 15 min). Subsequently, the supernatant and pellet fractions were loaded on SDS gel. Note that high salt and direct incubation at 95˚C do not dissociate PHFs, since the pellet at these conditions contained most of the protein. However, treatment by GdnHCl efficiently dissolves PHFs as most of the protein appears in the supernatant.

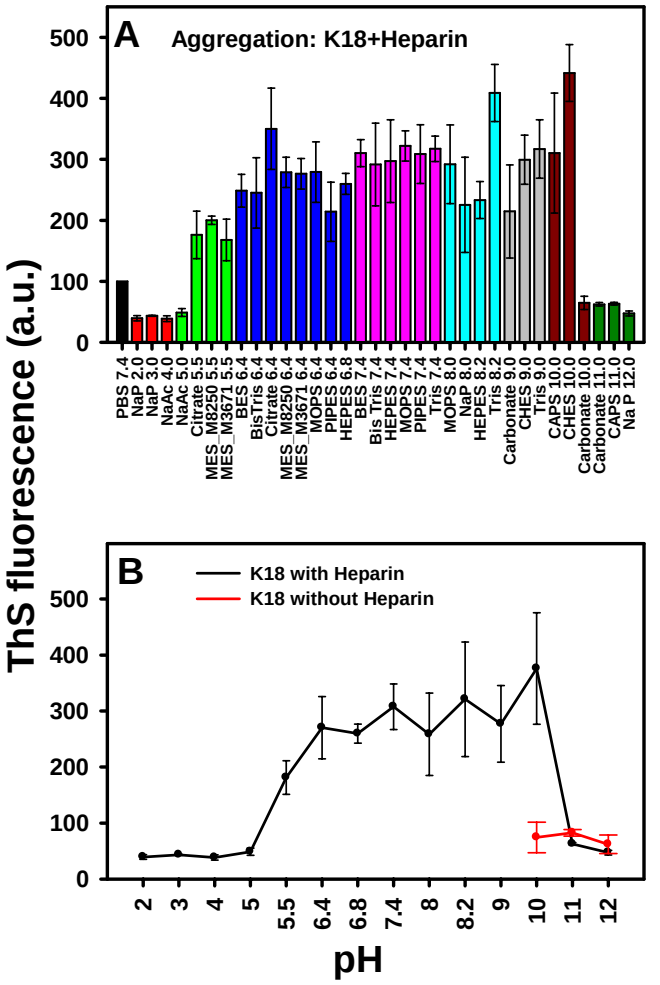

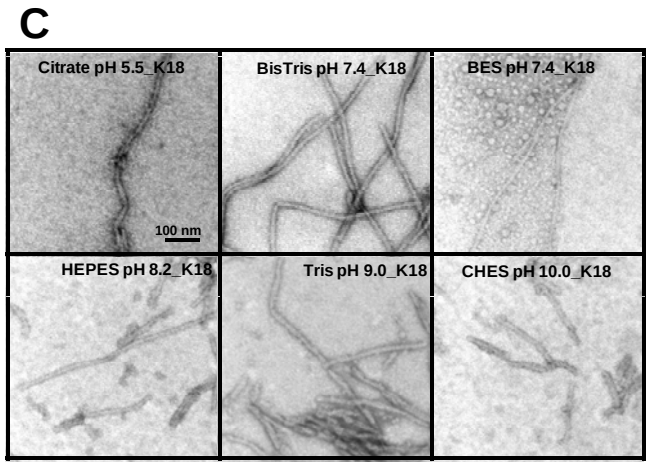

Supplementary figure 1

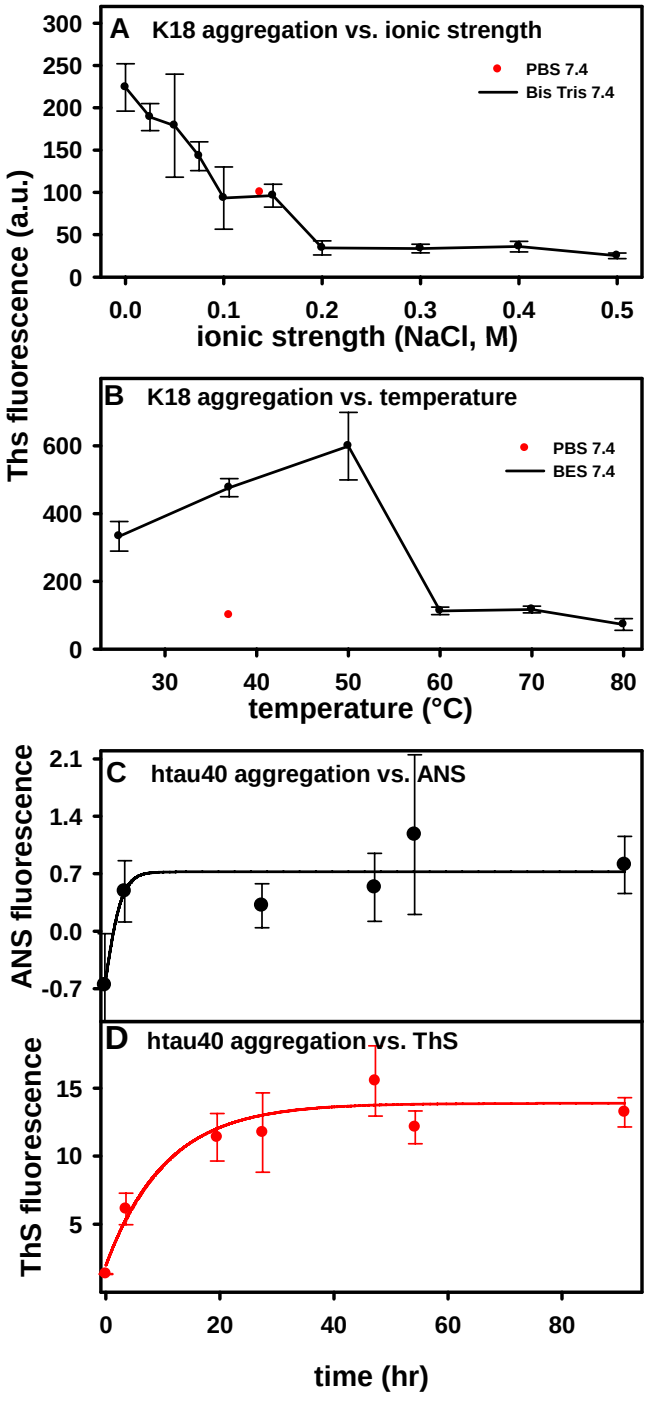

Supplementary figure 2

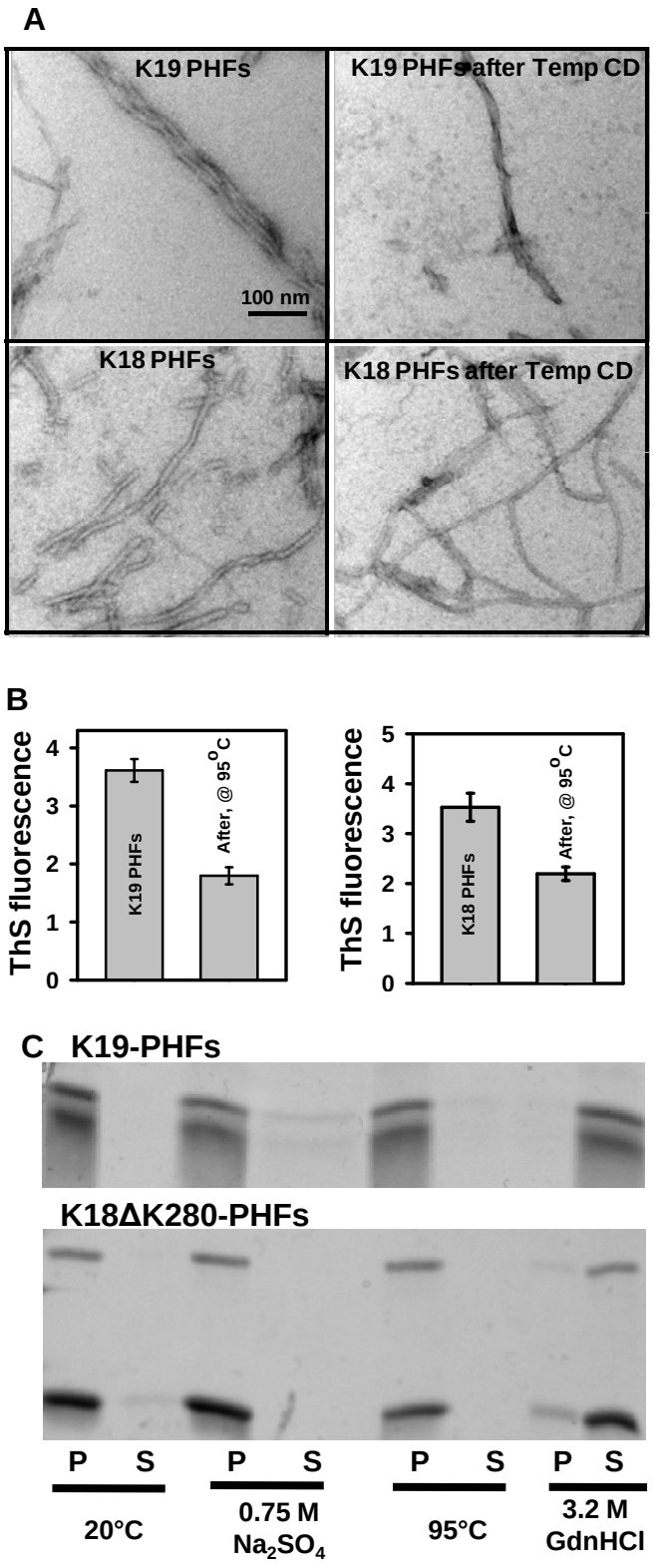

Supplementary figure 3